Journal of Advances in Mathematics and Computer Science

26(4): 1-26, 2018; Article no.JAMCS.39632
ISSN: 2456-9968
(Past name: British Journal of Mathematics & Computer Science, Past ISSN: 2231-0851)

Conservation Properties of the Trapezoidal Rule for Linear Transient Electromagnetics

Arup Nandy[1*] and C. S. Jog[2]

[1] *Department of Mechanical Engineering, Indian Institute of Technology, Guwahati, 781039, India.*
[2] *Department of Mechanical Engineering, Indian Institute of Science, Bangalore, 560012, India.*

Authors' contributions

This work was carried out in collaboration between both authors. Both authors read and approved the final manuscript.

Article Information

DOI: 10.9734/JAMCS/2018/39632
Editor(s):
(1) Dragos-Patru Covei, Professor, Department of Applied Mathematics, The Bucharest University of Economic Studies, Piata Romana, Romania.
Reviewers:
(1) Aliyu Bhar Kisabo, Nigeria.
(2) G. Y. Sheu, Chang-Jung Christian University Feng-Chia University, Taiwan.
Complete Peer review History: http://www.sciencedomain.org/review-history/23334

Original Research Article

Received: 13th December 2017
Accepted: 14th February 2018
Published: 26th February 2018

Abstract

The Time Domain Finite Element Method (TDFEM) has been used extensively to solve transient electromagnetic radiation and scattering problems. But in most implementations so far, vector basis functions have been used to discretize the field variables. In multiphysics simulations that involve coupling the electromagnetic equations with structural or fluid flow equations, nodal finite elements can provide a unified data structure for a monolithic coupled formulation. With such multiphysics simulations in view, in this work we develop a time-stepping strategy to model electromagnetic radiation and scattering within the nodal finite element framework. Although conservation of energy is well-known, we show in this work that there are additional quantities that are also conserved in the absence of loading. We then show that the developed time-stepping strategy (which is closely related to the trapezoidal rule that is widely used for solving linear hyperbolic problems) mimics these continuum conservation properties either exactly or to a very good approximation. Thus, the developed numerical strategy can be said to be 'unconditionally

**Corresponding author: E-mail: arupn@iitg.ernet.in*

stable' (from an energy perspective) allowing the use of arbitrarily large time-steps. The developed method uses standard elements with Lagrange interpolation functions and standard Gaussian quadrature. We demonstrate the high accuracy and robustness of the developed method for solving both interior and exterior domain radiation problems, and for finding the scattered field from conducting and dielectric bodies.

Keywords: Electromagnetic radiation and scattering; Time domain; Trapezoidal rule; Nodal finite elements.

1 Introduction

One of the most popular methods for conducting transient electromagnetic analysis is the Finite Difference Time Domain (FDTD) method introduced by Yee [1]. The most important reasons for its popularity are its programming simplicity, its minimum bookkeeping complexity, and the simplicity of its numerical integration algorithm [2]. The Time Domain Finite Element Method (TDFEM) [3]–[17] offers some advantages over the standard FDTD method, the most obvious one being its ability to deal with unstructured grids, allowing versatility in modeling complex geometries. There are two different approaches that are followed within TDFEM. In the first approach [3]–[11], one of the field variables is eliminated from the set of Maxwell equations resulting in a second-order vector wave equation, which is subsequently used to develop the variational formulation. Thus, either the electric or magnetic field is the only unknown field-variable that is discretized and solved for. The other field is obtained through postprocessing. In the other approach [11]–[17], two coupled first-order Maxwell equations are simultaneously used to develop the variational formulation. Mixed set of basis functions are used to discretize and solve for both the electric and magnetic fields simultaneously. The transient analysis of electromagnetic radiation and scattering in two dimensions is modelled assuming either z-polarized $\boldsymbol{E}$ field [18], [19] or z-polarized $\boldsymbol{H}$ field [20], [21].

For the solution of time domain electromagnetic radiation and scattering problems in unbounded domains, yet another powerful method is the Finite Element Boundary Integral (FEBI) method [6]–[19]. In this method, the infinite solution domain is divided into interior and exterior regions by an artificial boundary. The boundary integral method is used to model the exterior field, whereas in the interior domain a finite element method is used. On the artificial boundary, field continuity is enforced to couple these two representations. For large scale transient electromagnetic problems, the entire domain is divided in several subdomains, and subsequently, either the discontinuous Galerkin [22]–[24] or the domain decomposition method [25]–[27] is used. Subdomains are related to each other by equivalent surface currents.

In most of the TDFEM works [3]–[17], vector basis functions are used to discretize the field variable. In [13], [14], [16], edge elements are used to discretize the electric field. There are relatively few works [18], [28] within the TDFEM framework where nodal finite elements are used. In [18], two first-order coupled equations are solved within a two-dimensional nodal framework. In [28], a second-order equation is solved using integral lumping which allows the use of an explicit time integration scheme with the time-step size required to be below the limiting value required for stability.

In [29] a family of unconditionally stable algorithm is presented within the FDTD framework where the time evolution operator of the EM field is the exponential of a skewsymmetric matrix. Orthogonal approximation of this operator leads to unconditional stability. In [30], two energy-conserving methods are proposed within the FDTD framework. For time discretization, for the coupled set of first order equations, a leapfrog strategy is used [15]–[17], while in the case of the second-order TDFEM, central difference is used [6], [7], [10]. In order to suppress low frequency spurious responses the Newmark formulation is modified in [9]. Rieben et. al. [17] have presented

a strategy where energy is conserved in a time-averaged sense.

It is well known that in linear elastodynamics, the linear and angular momenta, and the total energy (in an undamped system) are conserved in the absence of body forces and tractions on the entire boundary. It was shown in [31] that the trapezoidal rule mimics these continuum conservation properties, and is thus, in some sense an 'optimal' strategy for linear hyperbolic problems. Regarding electromagnetic problems, it is well known that the total energy is conserved for interior domain problems in the absence of any current or charge. In this work, we show (for perhaps the first time) that, analogous to the linear and angular momenta in linear elastodynamics, there are additional conservation laws that the electric and magnetic fields obey. Furthermore, we develop a time-stepping strategy within a nodal finite element framework (that is similar to the trapezoidal rule in the structural context) that mimics either exactly or to a very close approximation these continuum conservation properties. Thus, the developed strategy can be said to be unconditionally stable (from an energy perspective) [32], [33]. In Section 3, we demonstrate by means of a numerical example also that the solution remains stable even with the use of a very large time step.

Although the implementation of the trapezoidal rule is relatively straightforward in the case of structural or acoustic problems, it is not so in the case of electromagnetic problems, where material discontinuities and sharp corners and edges pose severe problems of convergence to the correct solution within the context of the nodal finite element method [11]. To account for material discontinuities, we use a potential formulation along the same lines as in [34], [35].

The outline of the remainder of the article is as follows. In section 2, we derive the conservation laws (including the energy conservation law) for the electric and magnetic fields followed by the variational and finite element formulations. The additional considerations that are required to tackle scattering from conducting and dielectric bodies are also presented. Section 3 presents examples ranging from radiation in interior and exterior domains to scattering from conducting and dielectric bodies in order to demonstrate the robustness of the proposed method.

2 Mathematical Formulation

We will often use the following vector identity. If $\boldsymbol{a}$ and $\boldsymbol{b}$ are vectors, then

$$\boldsymbol{\nabla} \cdot (\boldsymbol{a} \times \boldsymbol{b}) = (\boldsymbol{\nabla} \times \boldsymbol{a}) \cdot \boldsymbol{b} - \boldsymbol{a} \cdot (\boldsymbol{\nabla} \times \boldsymbol{b}). \tag{2.1}$$

The governing equations for transient electromagnetics (in the absence of charge) are given by

$$\frac{\partial \boldsymbol{H}}{\partial t} + \frac{1}{\mu} \boldsymbol{\nabla} \times \boldsymbol{E} = \boldsymbol{0}, \tag{2.2}$$

$$\epsilon \frac{\partial \boldsymbol{E}}{\partial t} - \boldsymbol{\nabla} \times \boldsymbol{H} = -\boldsymbol{j}, \tag{2.3}$$

$$\boldsymbol{\nabla} \cdot (\mu \boldsymbol{H}) = 0, \tag{2.4}$$

$$\boldsymbol{\nabla} \cdot (\epsilon \boldsymbol{E}) = 0, . \tag{2.5}$$

where $\boldsymbol{E}$ and $\boldsymbol{H}$ are the electric and magnetic fields, $\boldsymbol{j}$ is the current density, ϵ and μ are the electric permittivity and magnetic permeability, respectively, $\epsilon_r = \epsilon/\epsilon_0$ and $\mu_r = \mu/\mu_0$ are the relative permittivity and relative permeability, where ϵ_0 and μ_0 represent the permittivity and permeability for vacuum, $k = k_0\sqrt{\mu_r \epsilon_r}$ is the wave number of the medium, $k_0 = \omega/c_0$ is the wave number of vacuum, ω is the frequency of excitation (in the special case of harmonic excitation) and $c_0 = 1/\sqrt{\epsilon_0 \mu_0}$ is the wave speed in vacuum.

2.1 Conservation properties of the Maxwell equations

Throughout the following discussion, we assume ϵ and μ to be piecewise constant over the domain Ω, and the domain itself to be unchanging with respect to time. The surface Γ is assumed to be the union $\Gamma_e \cup \Gamma_h$, where $\boldsymbol{E} \times \boldsymbol{n}$ is prescribed on Γ_e and $\boldsymbol{H} \times \boldsymbol{n}$ is prescribed on Γ_h. Integrating Eqn. (2.3) over the domain, we get

$$\frac{d}{dt}\int_\Omega \epsilon \boldsymbol{E}\, d\Omega = -\int_\Omega \boldsymbol{j}\, d\Omega + \int_\Gamma \boldsymbol{n} \times \boldsymbol{H}\, d\Gamma. \tag{2.6}$$

Assume that $\Gamma = \Gamma_h$, and that $\boldsymbol{H} \times \boldsymbol{n} = \boldsymbol{0}$ on Γ_h. Also assume $\boldsymbol{j} = \boldsymbol{0}$. Then from Eqn. (2.6) we get

$$\int_\Omega \epsilon \boldsymbol{E}\, d\Omega = \text{constant}. \tag{2.7}$$

i.e., in the absence of loading, $\int_\Omega \epsilon \boldsymbol{E}\, d\Omega$ is conserved. In a similar fashion, if we integrate Eqn. (2.2) over the domain, we get

$$\frac{d}{dt}\int_\Omega \mu \boldsymbol{H}\, d\Omega = \int_\Gamma \boldsymbol{E} \times \boldsymbol{n}\, d\Gamma. \tag{2.8}$$

Now, if $\Gamma = \Gamma_e$ and if $\boldsymbol{E} \times \boldsymbol{n} = \boldsymbol{0}$ on Γ_e, then from Eqn. (2.8), we get

$$\int_\Omega \mu \boldsymbol{H}\, d\Omega = \text{constant}. \tag{2.9}$$

Next take the dot product of Eqn. (2.3) with the position vector $\boldsymbol{x}$ and integrate over the domain. Using the vector identity given by Eqn. (2.1), and the fact that $\boldsymbol{\nabla} \times \boldsymbol{x} = \boldsymbol{0}$, we get

$$\begin{aligned}\frac{d}{dt}\int_\Omega \epsilon(\boldsymbol{x} \cdot \boldsymbol{E})\, d\Omega &= -\int_\Omega \boldsymbol{x} \cdot \boldsymbol{j}\, d\Omega - \int_\Gamma (\boldsymbol{x} \times \boldsymbol{H}) \cdot \boldsymbol{n}\, d\Gamma \\ &= -\int_\Omega \boldsymbol{x} \cdot \boldsymbol{j}\, d\Omega - \int_\Gamma (\boldsymbol{H} \times \boldsymbol{n}) \cdot \boldsymbol{x}\, d\Gamma.\end{aligned}$$

Thus, if $\boldsymbol{j} = \boldsymbol{0}$ and if $\boldsymbol{H} \times \boldsymbol{n} = \boldsymbol{0}$ on the entire boundary, we get

$$\int_\Omega \epsilon(\boldsymbol{x} \cdot \boldsymbol{E})\, d\Omega = \text{constant}. \tag{2.10}$$

i.e., $\int_\Omega \epsilon(\boldsymbol{x} \cdot \boldsymbol{E})\, d\Omega$ is conserved. In a similar fashion, we take the dot product of Eqn. (2.2) with $\boldsymbol{x}$ and integrate over the domain. Then we have,

$$\frac{d}{dt}\int_\Omega \mu(\boldsymbol{x} \cdot \boldsymbol{H})\, d\Omega = \int_\Gamma (\boldsymbol{E} \times \boldsymbol{n}) \cdot \boldsymbol{x}\, d\Gamma$$

Now, if $\Gamma = \Gamma_e$ and if $\boldsymbol{E} \times \boldsymbol{n} = \boldsymbol{0}$ on Γ_e, then

$$\int_\Omega \mu(\boldsymbol{x} \cdot \boldsymbol{H})\, d\Omega = \text{constant}. \tag{2.11}$$

i.e., $\int_\Omega \mu(\boldsymbol{x} \cdot \boldsymbol{H})\, d\Omega$ is conserved.

Now take the dot product of Eqn. (2.3) with $\boldsymbol{E}$, integrate over the domain and again use Eqn. (2.1) to get

$$\begin{aligned}\frac{d}{dt}\int_\Omega \frac{\epsilon}{2}(\boldsymbol{E} \cdot \boldsymbol{E})\, d\Omega &= -\int_\Omega \boldsymbol{E} \cdot \boldsymbol{j}\, d\Omega + \int_\Omega (\boldsymbol{\nabla} \times \boldsymbol{E}) \cdot \boldsymbol{H}\, d\Omega - \int_\Gamma (\boldsymbol{E} \times \boldsymbol{H}) \cdot \boldsymbol{n}\, d\Gamma \\ &= -\int_\Omega \boldsymbol{E} \cdot \boldsymbol{j}\, d\Omega - \frac{d}{dt}\int_\Omega \frac{\mu}{2}(\boldsymbol{H} \cdot \boldsymbol{H})\, d\Omega + \int_\Gamma (\boldsymbol{H} \times \boldsymbol{n}) \cdot [(\boldsymbol{E} \times \boldsymbol{n}) \times \boldsymbol{n}]\, d\Gamma.\end{aligned} \tag{2.12}$$

Thus, in the absence of loading $\boldsymbol{j}$, and if $\boldsymbol{E} \times \boldsymbol{n} = \boldsymbol{0}$ on Γ_e and $\boldsymbol{H} \times \boldsymbol{n} = \boldsymbol{0}$ on Γ_h, then we get

$$\int_\Omega \frac{1}{2} \left[\epsilon(\boldsymbol{E} \cdot \boldsymbol{E}) + \mu(\boldsymbol{H} \cdot \boldsymbol{H})\right] \, d\Omega = \text{constant}. \tag{2.13}$$

i.e., $\int_\Omega \frac{1}{2} \left[\epsilon(\boldsymbol{E} \cdot \boldsymbol{E}) + \mu(\boldsymbol{H} \cdot \boldsymbol{H})\right] \, d\Omega$ is conserved.

To summarize, in the absence of loading $\boldsymbol{j}$, the following quantities are conserved:

$$\bar{\boldsymbol{D}} = \int_\Omega \epsilon \boldsymbol{E} \, d\Omega, \qquad (\boldsymbol{H} \times \boldsymbol{n} = \boldsymbol{0} \text{ on the entire boundary}) \tag{2.14a}$$

$$\bar{\boldsymbol{B}} = \int_\Omega \mu \boldsymbol{H} \, d\Omega, \qquad (\boldsymbol{E} \times \boldsymbol{n} = \boldsymbol{0} \text{ on the entire boundary}) \tag{2.14b}$$

$$\alpha = \int_\Omega \epsilon(\boldsymbol{x} \cdot \boldsymbol{E}) \, d\Omega, \qquad (\boldsymbol{H} \times \boldsymbol{n} = \boldsymbol{0} \text{ on the entire boundary}) \tag{2.14c}$$

$$\beta = \int_\Omega \mu(\boldsymbol{x} \cdot \boldsymbol{H}) \, d\Omega, \qquad (\boldsymbol{E} \times \boldsymbol{n} = \boldsymbol{0} \text{ on the entire boundary}) \tag{2.14d}$$

$$\bar{E} = \int_\Omega \frac{1}{2} \left[\epsilon(\boldsymbol{E} \cdot \boldsymbol{E}) + \mu(\boldsymbol{H} \cdot \boldsymbol{H})\right] \, d\Omega, \qquad (\boldsymbol{E} \times \boldsymbol{n} = \boldsymbol{0} \text{ on } \Gamma_e \text{ and } \boldsymbol{H} \times \boldsymbol{n} = \boldsymbol{0} \text{ on } \Gamma_h), \tag{2.14e}$$

with the field $\boldsymbol{E}$ also satisfying the constraint $\boldsymbol{\nabla} \cdot \boldsymbol{E} = 0$. Although the conservation of $\bar{E}$ in Eqn. (2.14e) is well-known, the conservation of the other quantities in Eqns. (2.14) appears not to have been noted before.

2.2 Variational and FEM formulations

Our goal is to devise a numerical strategy that mimics the (continuum) conservation properties listed in Eqns. (2.14) within the context of the $\boldsymbol{A}$-ψ potential formulation. Let $\boldsymbol{v} := \partial \boldsymbol{A}/\partial t$ and $\boldsymbol{w} := \partial(\boldsymbol{\nabla}\psi)/\partial t$. In the $\boldsymbol{A}$-ψ formulation, we take

$$\boldsymbol{E} = -\boldsymbol{w} - \boldsymbol{v}, \tag{2.15}$$

$$\boldsymbol{H} = \frac{1}{\mu} \boldsymbol{\nabla} \times \boldsymbol{A}. \tag{2.16}$$

Thus, since $\boldsymbol{\nabla}\psi \cdot \boldsymbol{n}$ is discontinuous while $\boldsymbol{\nabla}\psi \times \boldsymbol{n}$ is continuous at the interface, we get the desired tangential continuity of the $\boldsymbol{E}$ field at a material interface. We use the gage condition $\boldsymbol{\nabla} \cdot \boldsymbol{A} = 0$. Using Eqns. (2.15) and (2.16), we see that Eqns. (2.2) and (2.4) are automatically satisfied, while Eqns. (2.3) and (2.5) reduce to

$$\epsilon \left[\frac{\partial^2 \boldsymbol{A}}{\partial t^2} + \boldsymbol{\nabla} \left(\frac{\partial^2 \psi}{\partial t^2}\right)\right] + \boldsymbol{\nabla} \times \left(\frac{1}{\mu} \boldsymbol{\nabla} \times \boldsymbol{A}\right) = \boldsymbol{j}, \tag{2.17}$$

$$\boldsymbol{\nabla} \cdot \left[\epsilon(\boldsymbol{\nabla}\dot{\psi} + \dot{\boldsymbol{A}})\right] = 0, \tag{2.18}$$

where superposed dots indicate time derivatives. Using Eqn. (2.1), the variational formulation is given by

$$\begin{aligned} &\int_\Omega \epsilon \boldsymbol{A}_\delta \cdot \left[\frac{\partial^2 \boldsymbol{A}}{\partial t^2} + \frac{\partial^2 (\boldsymbol{\nabla}\psi)}{\partial t^2}\right] \, d\Omega + \int_\Omega \frac{1}{\mu} (\boldsymbol{\nabla} \times \boldsymbol{A}_\delta) \cdot (\boldsymbol{\nabla} \times \boldsymbol{A}) \, d\Omega \\ &+ \int_\Omega \frac{1}{\mu} (\boldsymbol{\nabla} \cdot \boldsymbol{A}_\delta)(\boldsymbol{\nabla} \cdot \boldsymbol{A}) \, d\Omega = \int_\Omega \boldsymbol{A}_\delta \cdot \boldsymbol{j} \, d\Omega + \int_{\Gamma_h} \boldsymbol{A}_\delta \cdot \bar{\boldsymbol{H}} \, d\Gamma, \end{aligned} \tag{2.19}$$

$$\int_\Omega \epsilon(\boldsymbol{\nabla}\psi_\delta) \cdot \left[\dot{\boldsymbol{A}} + \boldsymbol{\nabla}\dot{\psi}\right] \, d\Omega = \int_\Gamma \psi_\delta \epsilon [(\dot{\boldsymbol{A}} + \boldsymbol{\nabla}\dot{\psi}) \cdot \boldsymbol{n}] \, d\Gamma, \tag{2.20}$$

where we have added a penalty term in the above variational form to enforce the gage constraint on $\boldsymbol{A}$ [34], [36]. The quantity $\bar{\boldsymbol{H}} = \boldsymbol{H} \times \boldsymbol{n}$ is prescribed on Γ_h.

It is well known that the above formulation fails to capture the singular fields in non-convex domains with sharp corners and edges. Costabel et. al. [37] suggest a strategy where the penalty factor associated with the regularization term varies with the distance from the corner or edge, while Otin [38], [39] uses a zero penalty in the layers adjacent to corners and edges. We modify the latter strategy as in [36], whereby we surround the entire nonconvex radiator/scatterer by a thin layer of elements with zero penalty, and use a nonzero penalty in the remaining domain.

2.3 Time-stepping strategy

We propose the following time-stepping strategy over a time interval $[t_n, t_{n+1}]$ with $t_\Delta := t_{n+1} - t_n$:

$$\frac{\boldsymbol{v}_n + \boldsymbol{v}_{n+1}}{2} = \frac{\boldsymbol{A}_{n+1} - \boldsymbol{A}_n}{t_\Delta}, \tag{2.21}$$

$$\frac{\boldsymbol{w}_n + \boldsymbol{w}_{n+1}}{2} = \frac{\boldsymbol{\nabla}\psi_{n+1} - \boldsymbol{\nabla}\psi_n}{t_\Delta}, \tag{2.22}$$

$$\begin{aligned}
&\int_\Omega \epsilon \boldsymbol{A}_\delta \cdot \left[\frac{\boldsymbol{v}_{n+1} - \boldsymbol{v}_n}{t_\Delta} + \frac{\boldsymbol{w}_{n+1} - \boldsymbol{w}_n}{t_\Delta} \right] d\Omega + \int_\Omega \frac{1}{\mu} (\boldsymbol{\nabla} \times \boldsymbol{A}_\delta) \cdot \left[\frac{\boldsymbol{\nabla} \times \boldsymbol{A}_n + \boldsymbol{\nabla} \times \boldsymbol{A}_{n+1}}{2} \right] d\Omega \\
&\quad + \int_\Omega \frac{1}{\mu} (\boldsymbol{\nabla} \cdot \boldsymbol{A}_\delta) \left[\frac{\boldsymbol{\nabla} \cdot \boldsymbol{A}_n + \boldsymbol{\nabla} \cdot \boldsymbol{A}_{n+1}}{2} \right] d\Omega \\
&\quad = \int_\Omega \boldsymbol{A}_\delta \cdot \left(\frac{1}{2} \int_{-1}^{1} \boldsymbol{j}(\bar{t})\, d\xi \right) d\Omega + \int_{\Gamma_h} \boldsymbol{A}_\delta \cdot \left(\frac{1}{2} \int_{-1}^{1} \bar{\boldsymbol{H}}(\bar{t})\, d\xi \right) d\Gamma,
\end{aligned} \tag{2.23}$$

$$\begin{aligned}
&\int_\Omega \epsilon (\boldsymbol{\nabla}\psi_\delta) \cdot (\boldsymbol{A}_{n+1} + \boldsymbol{\nabla}\psi_{n+1})\, d\Omega + \int_\Gamma \psi_\delta \epsilon\, (\boldsymbol{A}_n + \boldsymbol{\nabla}\psi_n) \cdot \boldsymbol{n}\, d\Gamma \\
&\quad = \int_\Omega \epsilon (\boldsymbol{\nabla}\psi_\delta) \cdot (\boldsymbol{A}_n + \boldsymbol{\nabla}\psi_n)\, d\Omega + \int_\Gamma \psi_\delta \epsilon\, (\boldsymbol{A}_{n+1} + \boldsymbol{\nabla}\psi_{n+1}) \cdot \boldsymbol{n}\, d\Gamma,
\end{aligned} \tag{2.24}$$

where $\bar{t} = \left(\frac{1-\xi}{2}\right) t_n + \left(\frac{1+\xi}{2}\right) t_{n+1}$. The loading terms in Eqn. (2.23) have been formulated in a way consistent with the linear time finite element method as presented in [40].

We now prove that the above time-stepping strategy conserves the quantities in Eqn. (2.14) in the absence of loading. Choose $\boldsymbol{A}_\delta = \boldsymbol{c}$, where $\boldsymbol{c}$ is a vector dependent only on time. Then Eqn. (2.23) in the absence of loading reduces to

$$\boldsymbol{c} \cdot \int_\Omega \epsilon \left[\boldsymbol{v}_{n+1} - \boldsymbol{v}_n + \boldsymbol{w}_{n+1} - \boldsymbol{w}_n \right] d\Omega = 0.$$

Since $\boldsymbol{c}$ is arbitrary, we get

$$\int_\Omega \epsilon \left[\boldsymbol{v}_{n+1} + \boldsymbol{w}_{n+1} \right] d\Omega = \int_\Omega \epsilon \left[\boldsymbol{v}_n + \boldsymbol{w}_n \right] d\Omega,$$

or, alternatively, $\int_\Omega \epsilon \boldsymbol{E}_{n+1}\, d\Omega = \int_\Omega \epsilon \boldsymbol{E}_n\, d\Omega$. Thus, the quantity in Eqn. (2.14a) is conserved.

Next, choose $\boldsymbol{A}_\delta = \boldsymbol{x}$. Then, since $\boldsymbol{\nabla} \times \boldsymbol{x} = \boldsymbol{0}$, Eqn. (2.23) in the absence of loading reduces to

$$\int_\Omega \epsilon \boldsymbol{x} \cdot \left[\boldsymbol{v}_{n+1} - \boldsymbol{v}_n + \boldsymbol{w}_{n+1} - \boldsymbol{w}_n \right] d\Omega + 3 t_\Delta \int_\Omega \frac{1}{2\mu} \boldsymbol{\nabla} \cdot (\boldsymbol{A}_n + \boldsymbol{A}_{n+1})\, d\Omega = 0.$$

Although it is possible for $\int_\Omega \boldsymbol{\nabla} \cdot \boldsymbol{A}_{n+1}\, d\Omega$ to be nonzero, we find that it turns out to be zero in all the examples, so that $\int_\Omega \epsilon \boldsymbol{x} \cdot \boldsymbol{E}_{n+1}\, d\Omega = \int_\Omega \epsilon \boldsymbol{x} \cdot \boldsymbol{E}_n\, d\Omega$. Thus, the quantity in Eqn. (2.14c) is conserved.

The energy is not conserved exactly by the above algorithm (due to the presence of the penalty term), but nevertheless find that energy conservation is satisfied almost perfectly as we show by means of various numerical examples in Section 3.

For exterior domain problems, the first-order absorbing boundary condition on the spherical truncation surface Γ_∞ is given by

$$\boldsymbol{n} \times (\boldsymbol{\nabla} \times \boldsymbol{E}) + \sqrt{\epsilon\mu}\boldsymbol{n} \times \left(\boldsymbol{n} \times \frac{\partial \boldsymbol{E}}{\partial t} \right) = \boldsymbol{0}. \tag{2.25}$$

Assuming zero initial conditions, this can be written as

$$\boldsymbol{n} \times (\boldsymbol{\nabla} \times \boldsymbol{A}) + \sqrt{\epsilon\mu}\boldsymbol{n} \times [\boldsymbol{n} \times (\boldsymbol{w} + \boldsymbol{v})] = \boldsymbol{0}.$$

If R denotes the radius of Γ_∞, then $\boldsymbol{n} \times (\boldsymbol{n} \times \boldsymbol{v})$ is $O(1/R)$, while $\boldsymbol{n} \times (\boldsymbol{n} \times \boldsymbol{w})$ is $O(1/R^2)$, and, hence, can be neglected. For the scaler field ψ we impose following far-field condition:

$$\boldsymbol{\nabla}\psi \cdot \boldsymbol{n} = -\frac{\psi}{R}.$$

Thus, for unbounded domain-problems, Eqns. (2.23)–(2.24) get modified to

$$\begin{aligned}
&\int_\Omega \epsilon \boldsymbol{A}_\delta \cdot \left[\frac{\boldsymbol{v}_{n+1} - \boldsymbol{v}_n}{t_\Delta} + \frac{(\boldsymbol{\nabla}\psi)_{n+1} - (\boldsymbol{\nabla}\psi)_n}{t_\Delta} \right] d\Omega + \int_\Omega \frac{1}{\mu} (\boldsymbol{\nabla} \times \boldsymbol{A}_\delta) \cdot \left[\frac{\boldsymbol{\nabla} \times \boldsymbol{A}_n + \boldsymbol{\nabla} \times \boldsymbol{A}_{n+1}}{2} \right] d\Omega \\
&\quad + \int_\Omega \frac{1}{\mu} (\boldsymbol{\nabla} \cdot \boldsymbol{A}_\delta) \left(\frac{(\boldsymbol{\nabla} \cdot \boldsymbol{A})_n + (\boldsymbol{\nabla} \cdot \boldsymbol{A})_{n+1}}{2} \right) d\Omega = \int_\Omega \boldsymbol{A}_\delta \cdot \left(\frac{1}{2} \int_{-1}^{1} \boldsymbol{j}(\bar{t})\, d\xi \right) d\Omega \\
&\quad + \int_\Gamma \boldsymbol{A}_\delta \cdot \left(\frac{1}{2} \int_{-1}^{1} \bar{\boldsymbol{H}}(\bar{t})\, d\xi \right) d\Gamma - \int_{\Gamma_\infty} \sqrt{\frac{\epsilon}{\mu}} (\boldsymbol{n} \times \boldsymbol{A}_\delta) \cdot \left[\boldsymbol{n} \times \left(\frac{\boldsymbol{A}_{n+1} - \boldsymbol{A}_n}{t_\Delta} \right) \right] d\Gamma, \qquad (2.26) \\
&\int_\Omega \epsilon (\boldsymbol{\nabla}\psi_\delta) \cdot (\boldsymbol{A}_{n+1} - \boldsymbol{A}_n + \boldsymbol{\nabla}\psi_{n+1} - \boldsymbol{\nabla}\psi_n)\, d\Omega + \int_{\Gamma_\infty} \left[\frac{\epsilon}{R} \psi_\delta (\psi_{n+1} - \psi_n) - \epsilon \psi_\delta (\boldsymbol{A}_{n+1} - \boldsymbol{A}_n) \cdot \boldsymbol{n} \right] d\Gamma = \\
&\quad \int_\Gamma \psi_\delta \epsilon (\boldsymbol{A}_{n+1} - \boldsymbol{A}_n + \boldsymbol{\nabla}\psi_{n+1} - \boldsymbol{\nabla}\psi_n) \cdot \boldsymbol{n}\, d\Gamma, \qquad (2.27)
\end{aligned}$$

where Γ now represents all surfaces barring Γ_∞.

Let the fields and their variations in Eqns. (2.26)–(2.27) be interpolated as

$$\begin{aligned}
\boldsymbol{A} &= \boldsymbol{N}\hat{\boldsymbol{A}}, & \boldsymbol{A}_\delta &= \boldsymbol{N}\hat{\boldsymbol{A}}_\delta, \\
\boldsymbol{\nabla} \times \boldsymbol{A} &= \boldsymbol{B}\hat{\boldsymbol{A}}, & \boldsymbol{\nabla} \times \boldsymbol{A}_\delta &= \boldsymbol{B}\hat{\boldsymbol{A}}_\delta, \\
\boldsymbol{\nabla} \cdot \boldsymbol{A} &= \boldsymbol{B}_p\hat{\boldsymbol{A}}, & \boldsymbol{\nabla} \cdot \boldsymbol{A}_\delta &= \boldsymbol{B}_p\hat{\boldsymbol{A}}_\delta, \\
\psi &= \boldsymbol{N}_\psi\hat{\boldsymbol{\psi}}, & \psi_\delta &= \boldsymbol{N}_\psi\hat{\boldsymbol{\psi}}_\delta, \\
\boldsymbol{\nabla}\psi &= \boldsymbol{B}_\psi\hat{\boldsymbol{\psi}}, & \boldsymbol{\nabla}\psi_\delta &= \boldsymbol{B}_\psi\hat{\boldsymbol{\psi}}_\delta,
\end{aligned}$$

where $\hat{\boldsymbol{A}}$ and $\hat{\boldsymbol{\psi}}$ denote the nodal values of $\boldsymbol{A}$ and ψ, $\hat{\boldsymbol{A}}_\delta$ and $\hat{\boldsymbol{\psi}}_\delta$ denote their respective variations

and

$$\boldsymbol{N} = \begin{bmatrix} N_1 & 0 & 0 & N_2 & 0 & 0 & \dots \\ 0 & N_1 & 0 & 0 & N_2 & 0 & \dots \\ 0 & 0 & N_1 & 0 & 0 & N_2 & \dots \end{bmatrix},$$

$$\boldsymbol{B} = \begin{bmatrix} 0 & -\frac{\partial N_1}{\partial z} & \frac{\partial N_1}{\partial y} & 0 & -\frac{\partial N_2}{\partial z} & \frac{\partial N_2}{\partial y} & \dots \\ \frac{\partial N_1}{\partial z} & 0 & -\frac{\partial N_1}{\partial x} & \frac{\partial N_2}{\partial z} & 0 & -\frac{\partial N_2}{\partial x} & \dots \\ -\frac{\partial N_1}{\partial y} & \frac{\partial N_1}{\partial x} & 0 & -\frac{\partial N_2}{\partial y} & \frac{\partial N_2}{\partial x} & 0 & \dots \end{bmatrix},$$

$$\boldsymbol{B}_p = \begin{bmatrix} \frac{\partial N_1}{\partial x} & \frac{\partial N_1}{\partial y} & \frac{\partial N_1}{\partial z} & \frac{\partial N_2}{\partial x} & \frac{\partial N_2}{\partial y} & \frac{\partial N_2}{\partial z} & \dots \end{bmatrix},$$

$$\boldsymbol{N}_\psi = \begin{bmatrix} N_1 & N_2 & N_3 & \dots \end{bmatrix},$$

$$\boldsymbol{B}_\psi = \begin{bmatrix} \frac{\partial N_1}{\partial x} & \frac{\partial N_2}{\partial x} & \frac{\partial N_3}{\partial x} & \dots \\ \frac{\partial N_1}{\partial y} & \frac{\partial N_2}{\partial y} & \frac{\partial N_3}{\partial y} & \dots \\ \frac{\partial N_1}{\partial z} & \frac{\partial N_2}{\partial z} & \frac{\partial N_3}{\partial z} & \dots \end{bmatrix}.$$

Using the arbitrariness of the variations, we get

$$\begin{bmatrix} \boldsymbol{K}_{AA} & \boldsymbol{K}_{A\psi} \\ \boldsymbol{K}_{\psi A} & \boldsymbol{K}_{\psi\psi} \end{bmatrix} \begin{bmatrix} \hat{\boldsymbol{A}}_{n+1} \\ \hat{\boldsymbol{\psi}}_{n+1} \end{bmatrix} = \begin{bmatrix} \boldsymbol{f}_A \\ \boldsymbol{f}_\psi \end{bmatrix}, \tag{2.28}$$

where, with $\boldsymbol{n}_{\text{mat}}$ denoting the skew-symmetric matrix whose axial vector is $\boldsymbol{n}$,

$$\boldsymbol{K}_{AA} = \int_\Omega \left[\frac{2\epsilon}{t_\Delta^2} \boldsymbol{N}^T \boldsymbol{N} + \frac{1}{2\mu} \boldsymbol{B}^T \boldsymbol{B} + \frac{1}{2\mu} \boldsymbol{B}_p^T \boldsymbol{B}_p \right] d\Omega + \int_{\Gamma_\infty} \frac{1}{t_\Delta} \sqrt{\frac{\epsilon}{\mu}} \boldsymbol{N}^T \boldsymbol{n}_{\text{mat}} \boldsymbol{n}_{\text{mat}}^T \boldsymbol{N} \, d\Gamma,$$

$$\boldsymbol{K}_{A\psi} = \int_\Omega \frac{2\epsilon}{t_\Delta^2} \boldsymbol{N}^T \boldsymbol{B}_\psi \, d\Omega,$$

$$\boldsymbol{K}_{\psi A} = \int_\Omega \epsilon \boldsymbol{B}_\psi^T \boldsymbol{N} \, d\Omega - \int_\Gamma \epsilon \boldsymbol{N}_\psi^T \boldsymbol{n}^T \boldsymbol{N} \, d\Gamma - \int_{\Gamma_\infty} \epsilon \boldsymbol{N}_\psi^T \boldsymbol{n}^T \boldsymbol{N} \, d\Gamma,$$

$$\boldsymbol{K}_{\psi\psi} = \int_\Omega \epsilon \boldsymbol{B}_\psi^T \boldsymbol{B}_\psi \, d\Omega - \int_\Gamma \epsilon \boldsymbol{N}_\psi^T \boldsymbol{n}^T \boldsymbol{B}_\psi \, d\Gamma + \int_{\Gamma_\infty} \frac{\epsilon}{R} \boldsymbol{N}^T \boldsymbol{N} \, d\Gamma,$$

$$\begin{aligned} \boldsymbol{f}_A = {} & \int_\Gamma \boldsymbol{N}^T \left(\frac{1}{2} \int_{-1}^{1} \bar{\boldsymbol{H}}(\bar{t}) \, d\xi \right) d\Gamma + \int_\Omega \boldsymbol{N}^T \left[\left(\frac{1}{2} \int_{-1}^{1} \boldsymbol{j}(\bar{t}) \, d\xi \right) + \frac{2\epsilon}{t_\Delta^2} \boldsymbol{A}_n + \frac{2\epsilon}{t_\Delta} \boldsymbol{v}_n + \frac{2\epsilon}{t_\Delta^2} \boldsymbol{\nabla} \psi_n + \frac{2\epsilon}{t_\Delta} \boldsymbol{w}_n \right] d\Omega \\ & - \int_\Omega \frac{1}{2\mu} \left[\boldsymbol{B}^T (\boldsymbol{\nabla} \times \boldsymbol{A}_n) + \boldsymbol{B}_p^T (\boldsymbol{\nabla} \cdot \boldsymbol{A}_n) \right] d\Omega + \int_{\Gamma_\infty} \frac{1}{t_\Delta} \sqrt{\frac{\epsilon}{\mu}} \boldsymbol{N}^T \boldsymbol{n}_{\text{mat}} \boldsymbol{n}_{\text{mat}}^T \boldsymbol{A}_n \, d\Gamma, \end{aligned}$$

$$\boldsymbol{f}_\psi = \int_\Omega \epsilon \boldsymbol{B}_\psi^T (\boldsymbol{A}_n + \boldsymbol{\nabla} \psi_n) \, d\Omega - \int_\Gamma \epsilon \boldsymbol{N}_\psi^T \boldsymbol{n}^T (\boldsymbol{A}_n + \boldsymbol{\nabla} \psi_n) \, d\Gamma + \int_{\Gamma_\infty} \epsilon \boldsymbol{N}_\psi^T \left[\frac{\psi_n}{R} - \boldsymbol{n}^T \boldsymbol{A}_n \right] d\Gamma.$$

2.4 Axisymmetric formulation

An axisymmetric formulation in a cylindrical coordinate system (r, θ, z) can be given if the excitation and geometry in a radiation problem are axisymmetric. Let the excitation and geometry be such that $E_r = E_z = 0$ and $E_\theta = E_\theta(r, z)$. Corresponding to this, we have $H_\theta = 0$, and H_r and H_z are functions of r and z. Under these assumptions, $\boldsymbol{\nabla} \times \boldsymbol{E}$ has the following simple expression in the

r–θ–z system:

$$\boldsymbol{\nabla} \times \boldsymbol{E} = -\frac{\partial E_\theta}{\partial z}\hat{\boldsymbol{e}}_r + \left(\frac{E_\theta}{r} + \frac{\partial E_\theta}{\partial r}\right)\hat{\boldsymbol{e}}_z \tag{2.29}$$

Since the only nonzero component of $\boldsymbol{E}$ is tangential to the mesh in the r-z plane (in the out-of-plane direction), there is no discontinuity in the normal component of $\boldsymbol{E}$ at the surface of an inhomogeneity. Hence, there is no need to work with potentials, and we can work directly with $\boldsymbol{E}$ even for inhomogeneous domains. Furthermore, since $\boldsymbol{\nabla} \cdot \boldsymbol{E} = 0$ we do not even need to include the regularization term. Hence, the only equation that we need to consider is

$$\epsilon \frac{\partial^2 \boldsymbol{E}}{\partial t^2} + \boldsymbol{\nabla} \times \left(\frac{1}{\mu}\boldsymbol{\nabla} \times \boldsymbol{E}\right) + \frac{\partial \boldsymbol{j}}{\partial t} = \boldsymbol{0}.$$

The variational form can be written as

$$\begin{aligned}&\int_\Omega \epsilon \boldsymbol{E}_\delta \cdot \frac{\partial^2 \boldsymbol{E}}{\partial t^2}\, d\Omega + \int_\Omega \frac{1}{\mu}(\boldsymbol{\nabla} \times \boldsymbol{E}_\delta) \cdot (\boldsymbol{\nabla} \times \boldsymbol{E})\, d\Omega + \int_{\Gamma_\infty} \frac{1}{c\mu}(\boldsymbol{E}_\delta \times \boldsymbol{n}) \cdot \left(\frac{\partial \boldsymbol{E}}{\partial t} \times \boldsymbol{n}\right) d\Gamma = \\ &-\int_\Omega \boldsymbol{E}_\delta \cdot \frac{\partial \boldsymbol{j}}{\partial t}\, d\Omega - \int_{\Gamma_h} \boldsymbol{E}_\delta \cdot \frac{\partial \bar{\boldsymbol{H}}}{\partial t}\, d\Gamma,\end{aligned} \tag{2.30}$$

where $\bar{\boldsymbol{H}} = \boldsymbol{H} \times \boldsymbol{n}$ is prescribed on Γ_h, and on Γ_∞ we have the radiation condition given by (2.25). We propose the following time-stepping strategy for Eqn. (2.30):

$$\frac{\boldsymbol{v}_n + \boldsymbol{v}_{n+1}}{2} = \frac{\boldsymbol{E}_{n+1} - \boldsymbol{E}_n}{t_\Delta}, \tag{2.31a}$$

$$\begin{aligned}&\int_\Omega \epsilon \boldsymbol{E}_\delta \cdot \left(\frac{\boldsymbol{v}_{n+1} - \boldsymbol{v}_n}{t_\Delta}\right) d\Omega + \int_\Omega \frac{1}{\mu}(\boldsymbol{\nabla} \times \boldsymbol{E}_\delta) \cdot \left[\frac{\boldsymbol{\nabla} \times \boldsymbol{E}_n + \boldsymbol{\nabla} \times \boldsymbol{E}_{n+1}}{2}\right] d\Omega + \\ &\int_{\Gamma_\infty} \frac{1}{c\mu}(\boldsymbol{E}_\delta \times \boldsymbol{n}) \cdot \left(\frac{\boldsymbol{E}_{n+1} - \boldsymbol{E}_n}{t_\Delta} \times \boldsymbol{n}\right) d\Gamma = -\int_\Omega \boldsymbol{E}_\delta \cdot \left(\frac{\boldsymbol{j}_{n+1} - \boldsymbol{j}_n}{t_\Delta}\right) d\Omega - \int_{\Gamma_h} \boldsymbol{E}_\delta \cdot \left(\frac{\bar{\boldsymbol{H}}_{n+1} - \bar{\boldsymbol{H}}_n}{t_\Delta}\right) d\Gamma.\end{aligned} \tag{2.31b}$$

We discretize the different terms as

$$\begin{aligned} E_\theta &= \boldsymbol{N}\hat{\boldsymbol{E}}_\theta, & \boldsymbol{H} &= \bar{\boldsymbol{N}}\hat{\boldsymbol{H}}, \\ \boldsymbol{\nabla} \times \boldsymbol{E} &= \boldsymbol{B}\hat{\boldsymbol{E}}_\theta, & \boldsymbol{E} \times \boldsymbol{n} &= \hat{\boldsymbol{n}}\boldsymbol{N}\hat{\boldsymbol{E}}_\theta, \end{aligned}$$

with similar interpolations for the variations, where

$$\begin{aligned} \boldsymbol{N} &= \begin{bmatrix} N_1 & N_2 & \dots \end{bmatrix}, \\ \hat{\boldsymbol{n}}^T &= \begin{bmatrix} n_z & -n_r \end{bmatrix}, \\ \bar{\boldsymbol{N}} &= \begin{bmatrix} N_1 & 0 & N_2 & 0 & \dots \\ 0 & N_1 & 0 & N_2 & \dots \end{bmatrix}, \\ \boldsymbol{B} &= \begin{bmatrix} -\dfrac{\partial N_1}{\partial z} & -\dfrac{\partial N_2}{\partial z} & \dots \\ \dfrac{N_1}{r} + \dfrac{\partial N_1}{\partial r} & \dfrac{N_2}{r} + \dfrac{\partial N_2}{\partial r} & \dots \end{bmatrix}. \end{aligned} \tag{2.32}$$

For points on the axis $r = 0$, instead of the $\boldsymbol{B}$ matrix in Eqn. (2.32), we use the following matrix [36]

$$\boldsymbol{B} = \begin{bmatrix} -\dfrac{\partial N_1}{\partial z} & -\dfrac{\partial N_2}{\partial z} & \dots \\ 2\dfrac{\partial N_1}{\partial r} & 2\dfrac{\partial N_2}{\partial r} & \dots \end{bmatrix}. \tag{2.33}$$

After substituting the above discretizations into Eqns. (2.31) and eliminating $\hat{\boldsymbol{v}}_{n+1}$, we get

$$\boldsymbol{K}_{\text{axi}}\hat{\boldsymbol{E}}_{\theta_{n+1}} = \boldsymbol{f}_{\text{axi}},$$

where

$$\begin{aligned}
\boldsymbol{K}_{\text{axi}} &= \frac{2}{t_\Delta^2}\int_\Omega \epsilon r \boldsymbol{N}^T\boldsymbol{N}\,dr\,dz + \frac{1}{2}\int_\Omega \frac{r}{\mu}\boldsymbol{B}^T\boldsymbol{B}\,dr\,dz + \frac{1}{t_\Delta}\int_{\Gamma_\infty}\frac{r}{c\mu}\boldsymbol{N}^T\boldsymbol{N}\,ds,\\
\boldsymbol{f}_{\text{axi}} &= -\int_\Omega \boldsymbol{N}^T\left(\frac{\boldsymbol{j}_{n+1}-\boldsymbol{j}_n}{t_\Delta}\right)dr\,dz - \int_{\Gamma_h}\boldsymbol{N}^T\left(\frac{\bar{\boldsymbol{H}}_{n+1}-\bar{\boldsymbol{H}}_n}{t_\Delta}\right)ds + \frac{2}{t_\Delta^2}\int_\Omega \epsilon r\boldsymbol{N}^T E_{\theta_n}\,dr\,dz\\
&\quad - \frac{1}{2}\int_\Omega \frac{r}{\mu}\boldsymbol{B}^T(\boldsymbol{\nabla}\times\boldsymbol{E}_n)\,dr\,dz + \frac{1}{t_\Delta}\int_{\Gamma_\infty}\frac{r}{c\mu}\boldsymbol{N}^T E_{\theta_n}\,ds + \frac{2}{t_\Delta}\int_\Omega \epsilon r\boldsymbol{N}^T v_n\,dr\,dz,
\end{aligned}$$

where $ds = \sqrt{dr^2+dz^2}$. After solving for $\hat{\boldsymbol{E}}_{\theta_{n+1}}$, we can obtain $\boldsymbol{H}_{n+1}$ using

$$\boldsymbol{H}_{n+1} = \boldsymbol{H}_n - \frac{t_\Delta}{2\mu}(\boldsymbol{\nabla}\times\boldsymbol{E}_n + \boldsymbol{\nabla}\times\boldsymbol{E}_{n+1}).$$

2.5 Scattering from conducting and dielectric bodies

Consider an incident wave $\boldsymbol{E}_{\text{inc}}$ that impinges on a conducting or dielectric body. The total field is given by the sum of the incident and the scattered field, i.e., $\boldsymbol{E} = \boldsymbol{E}_{\text{scat}} + \boldsymbol{E}_{\text{inc}}$. In place of $\boldsymbol{E}$, the scattered field $\boldsymbol{E}_{\text{scat}}$ should satisfy Eqn. (2.25) on Γ_∞, i.e., on Γ_∞:

$$\boldsymbol{n}\times(\boldsymbol{\nabla}\times\boldsymbol{E}) + \sqrt{\epsilon\mu}\boldsymbol{n}\times\left(\boldsymbol{n}\times\frac{\partial\boldsymbol{E}}{\partial t}\right) = -\mu\boldsymbol{n}\times\frac{\partial\boldsymbol{H}_{\text{inc}}}{\partial t} + \sqrt{\epsilon\mu}\boldsymbol{n}\times\left(\boldsymbol{n}\times\frac{\partial\boldsymbol{E}_{\text{inc}}}{\partial t}\right). \tag{2.34}$$

Hence, for scattering from conducting and dielectric bodies, $\boldsymbol{f}_A$ in Eqn. (2.28) should be replaced by $\bar{\boldsymbol{f}}_A$ given by

$$\bar{\boldsymbol{f}}_A = \boldsymbol{f}_A - \int_{\Gamma_\infty}\left\{\boldsymbol{N}^T\boldsymbol{n}_{\text{mat}}\left(\frac{1}{2}\int_{-1}^{1}\boldsymbol{H}_{\text{inc}}(\bar{t})d\xi\right) + \sqrt{\frac{\epsilon}{\mu}}\boldsymbol{N}^T\boldsymbol{n}_{\text{mat}}\boldsymbol{n}_{\text{mat}}^T\left(\frac{1}{2}\int_{-1}^{1}\boldsymbol{E}_{\text{inc}}(\bar{t})d\xi\right)\right\}d\Gamma,$$

where $\bar{t} = \left(\frac{1-\xi}{2}\right)t_n + \left(\frac{1+\xi}{2}\right)t_{n+1}$.

For scattering from conducting bodies, in addition to satisfying the Maxwell equations, on the conducting surface we have to satisfy

$$\boldsymbol{E}\times\boldsymbol{n} = 0. \tag{2.35}$$

We enforce this constraint using a Lagrange multiplier technique. We follow the same time-stepping strategy as in Eqns. (2.22)–(2.24). Thus, for scattering from conducting bodies, Eqn. (2.28) gets modified to

$$\begin{bmatrix} \boldsymbol{K}_{AA} & \boldsymbol{K}_{A\psi} & \frac{1}{2}\int_{-1}^{1}\int_{-1}^{1}\boldsymbol{N}^T\boldsymbol{t}^T\boldsymbol{N}_\lambda d\xi d\eta \\ \boldsymbol{K}_{\psi A} & \boldsymbol{K}_{\psi\psi} & \boldsymbol{0} \\ \frac{1}{t_\Delta}\int_{-1}^{1}\int_{-1}^{1}\boldsymbol{N}_\lambda^T\boldsymbol{t}\boldsymbol{N}d\xi d\eta & \boldsymbol{0} & \boldsymbol{0} \end{bmatrix}\begin{bmatrix}\hat{\boldsymbol{A}}_{n+1}\\ \hat{\boldsymbol{\psi}}_{n+1}\\ \hat{\boldsymbol{\lambda}}_{n+1}\end{bmatrix} = \begin{bmatrix}\bar{\boldsymbol{f}}_A - \frac{1}{2}\int_{-1}^{1}\int_{-1}^{1}\boldsymbol{N}^T\boldsymbol{t}^T\boldsymbol{N}_\lambda\hat{\boldsymbol{\lambda}}_n d\xi d\eta\\ \boldsymbol{f}_\psi \\ \frac{1}{t_\Delta}\int_{-1}^{1}\int_{-1}^{1}\boldsymbol{N}_\lambda^T\boldsymbol{t}\boldsymbol{N}\hat{\boldsymbol{A}}_n d\xi d\eta\end{bmatrix}, \tag{2.36}$$

where $\boldsymbol{t}$ is a 2×3 matrix containing along its rows two linearly independent vectors $\boldsymbol{t}_1$ and $\boldsymbol{t}_2$ that are both perpendicular to the (unnormalized) normal $\bar{\boldsymbol{n}}$, (ξ,η) are natural coordinates that parameterize the surface of the element, and

$$\bar{\boldsymbol{n}} = \frac{\partial\boldsymbol{x}}{\partial\xi}\times\frac{\partial\boldsymbol{x}}{\partial\eta},$$

$$\boldsymbol{N}_\lambda = \begin{bmatrix} N_1 & 0 & N_2 & 0 & \dots \\ 0 & N_1 & 0 & N_2 & \dots \end{bmatrix}.$$

Note that the surface Jacobian in Eqn. (2.36) gets canceled and hence does not appear in the expressions. Since the Lagrange multiplier technique cannot handle abrupt changes in slope of the continuum (e.g., edges of a cube), the entire $\boldsymbol{A}$ vector along edges with a discontinuous normal $\boldsymbol{n}$ is set to zero, and the corresponding Lagrange multipliers are also suppressed.

For scattering from dielectric bodies, the material discontinuity leads to a discontinuity in $\boldsymbol{E} \cdot \boldsymbol{n}$ although $\boldsymbol{E} \times \boldsymbol{n}$ is continuous at the dielectric interface. This physical requirement is automatically taken care of by the assumed $\boldsymbol{A} - \psi$ form of $\boldsymbol{E}$ as in Eqn. (2.15).

3 Numerical Examples

In all the examples, we take $c = 3 \times 10^8 / \sqrt{\epsilon_r \mu_r}$ m/s.

3.1 Electromagnetic radiation inside a cube with conducting walls

Consider a cube of side-length π with conducting walls. The following solution (which is the transient counterpart of the harmonic problem described in [35]) exactly satisfies the governing equations and boundary conditions:

$$\begin{aligned}
E_x &= 2\cos(x)\sin(y)\sin(z)\left[\cos(\omega t) - \sin(\omega t)\right], \\
E_y &= \sin(x)\cos(y)\sin(z)\left[\sin(\omega t) - \cos(\omega t)\right], \\
E_z &= \sin(x)\sin(y)\cos(z)\left[\sin(\omega t) - \cos(\omega t)\right], \\
H_x &= 0, \\
H_y &= \frac{-3}{\mu\omega}\cos(x)\sin(y)\cos(z)\left[\cos(\omega t) + \sin(\omega t)\right], \\
H_z &= \frac{3}{\mu\omega}\cos(x)\cos(y)\sin(z)\left[\cos(\omega t) + \sin(\omega t)\right].
\end{aligned} \tag{3.1}$$

$$\begin{aligned}
A_x &= \frac{-2}{\omega}\cos(x)\sin(y)\sin(z)\left[\sin(\omega t) + \cos(\omega t)\right], \\
A_y &= \frac{1}{\omega}\sin(x)\cos(y)\sin(z)\left[\cos(\omega t) + \sin(\omega t)\right], \\
A_z &= \frac{1}{\omega}\sin(x)\sin(y)\cos(z)\left[\cos(\omega t) + \sin(\omega t)\right], \\
\psi &= 0, \\
j_x &= \left(\frac{2\epsilon\mu\omega^2 - 6}{\mu\omega}\right)\cos(x)\sin(y)\sin(z)\left[\cos(\omega t) + \sin(\omega t)\right], \\
j_y &= \left(\frac{3 - \epsilon\mu\omega^2}{\mu\omega}\right)\sin(x)\cos(y)\sin(z)\left[\cos(\omega t) + \sin(\omega t)\right], \\
j_z &= \left(\frac{3 - \epsilon\mu\omega^2}{\mu\omega}\right)\sin(x)\sin(y)\cos(z)\left[\cos(\omega t) + \sin(\omega t)\right].
\end{aligned} \tag{3.2}$$

The problem is solved with $\omega = 3 \times 10^8$ rad/s, applying $\boldsymbol{j}$ throughout the domain, and with initial $\boldsymbol{A}$ consistent with that in the solution given by Eqns. (3.1) and (3.2). We model the domain with a $4 \times 4 \times 4$ mesh of 27 node hexahedral elements. The time-step t_Δ is chosen to be 10^{-9} sec, and the time of simulation to be 4×10^{-8} sec. Fig. 1 shows the almost perfect match between the analytical (A) and FEM (F) time responses for the electric field components at two points $(x, y, z) = (\pi/4, \pi/8, 3\pi/4)$ and $(3\pi/4, \pi/4, \pi/8)$. Since $\boldsymbol{E} \times \boldsymbol{n} = \boldsymbol{0}$ on the entire boundary, the quantities $\bar{\boldsymbol{B}}$ and β should be conserved as per Eqns. (2.9) and (2.11). Fig. 2 shows that the

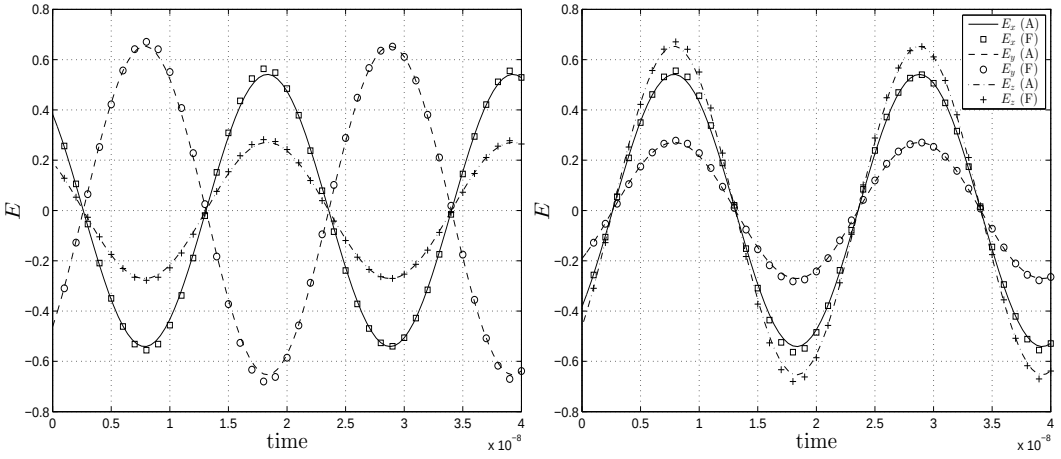

(a) $(x, y, z) = (\pi/4, \pi/8, 3\pi/4)$ (b) $(x, y, z) = (3\pi/4, \pi/4, \pi/8)$

Fig. 1. Time variation of the electric field for the cube with conducting walls example

proposed time-stepping strategy exactly mimics these conservation properties. Furthermore, after 4×10^{-8} sec, we set $\boldsymbol{j}$ to zero, i.e., after this time there is no external loading, and hence, as per Eqn. (2.13), $\bar{E}$ should be conserved. Fig. 2 shows that our numerical strategy conserves $\bar{E}$ after 4×10^{-8} sec, thus mimicking the continuum requirement.

3.2 Radiation problem inside a cube with prescribed $\boldsymbol{H}$ on the boundary

This problem is based on [41]. The analytical solution is given by

$$
\begin{aligned}
&E_x = \sin(\omega t - kz), && E_y = \sin(\omega t - kx), && E_z = \sin(\omega t - ky),\\
&H_x = \frac{k}{\mu\omega}\sin(\omega t - ky), && H_y = \frac{k}{\mu\omega}\sin(\omega t - kz), && H_z = \frac{k}{\mu\omega}\sin(\omega t - kx),\\
&j_x = \left(\frac{k^2}{\mu\omega} - \omega\epsilon\right)\cos(\omega t - kz), && j_y = \left(\frac{k^2}{\mu\omega} - \omega\epsilon\right)\cos(\omega t - kx), && j_z = \left(\frac{k^2}{\mu\omega} - \omega\epsilon\right)\cos(\omega t - ky),\\
&A_x = \frac{1}{\omega}\cos(\omega t - kz), && A_y = \frac{1}{\omega}\cos(\omega t - kx), && A_z = \frac{1}{\omega}\cos(\omega t - ky),\\
&\psi = 0.
\end{aligned}
$$

The problem is modelled with $\omega = 2$, $k = 3$, $\mu = 30/8$ and $\epsilon = 0.2$. A cube of dimension 2 is modelled with a mesh of $6 \times 6 \times 6$ elements of 27 node brick elements. The time-step is taken as 0.1 sec. Fig. 3 shows the almost perfect match between our FEM results (F) and the analytical solution (A). The result is shown upto 10 sec at two different points of the domain. After 10 sec $\boldsymbol{H} \times \boldsymbol{n}$ is set to zero and after 15 sec $\boldsymbol{j}$ is set to zero. From Fig. 4, we see that after 15 sec, $\bar{\boldsymbol{D}}$ and α are conserved exactly in accordance with Eqns. (2.14a) and (2.14c), while (due to the presence of the penalty term) conservation of $\bar{E}$ as per Eqn. (2.14e) is satisfied approximately. In order to demonstrate the stability of the algorithm, we use a time step that is twenty times that used previously, namely, 2 s, and also run the simulation for a much larger period, namely 100 s. Fig.

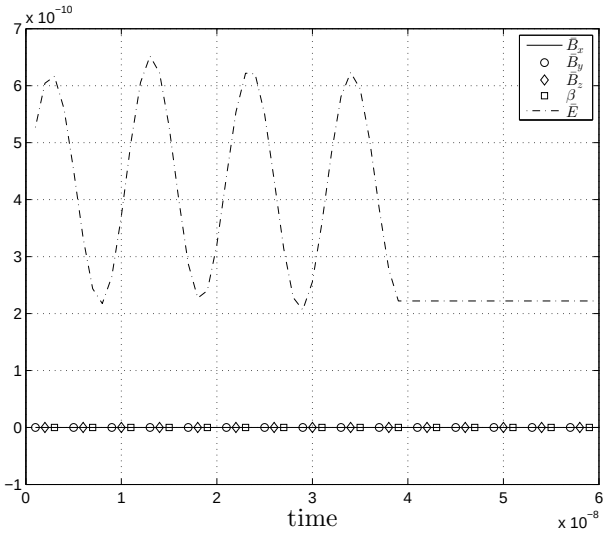

Fig. 2. Conservation of various quantities in the cube with conducting walls example

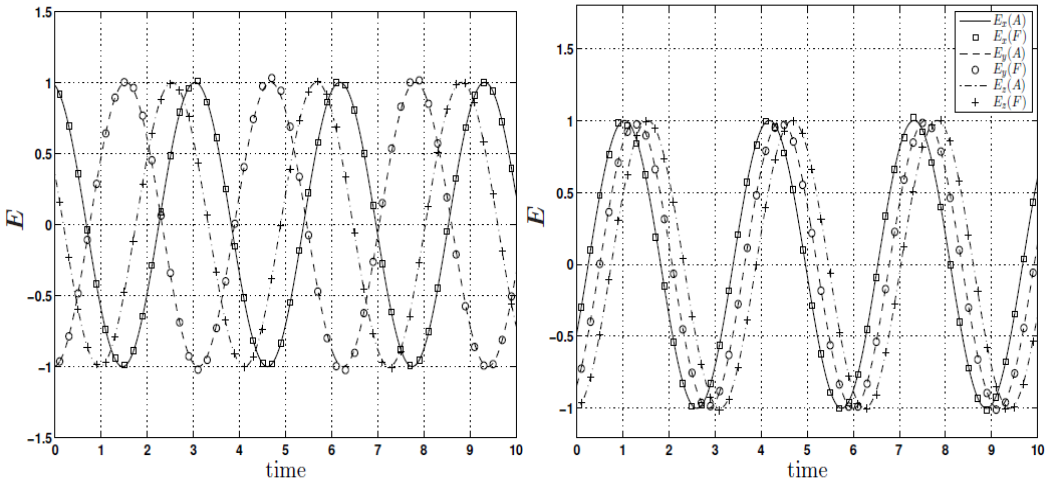

(a) $(x, y, z) = (1/2, 7/6, 3/2)$ (b) $(x, y, z) = (1/3, 1/2, 1/6)$

Fig. 3. Time variation of the electric field for the cube with boundary-prescribed H problem

5 shows the conservation of different quantities and the bounded nature of the solution. This is a numerical verification of the unconditionally stable nature of the proposed algorithm.

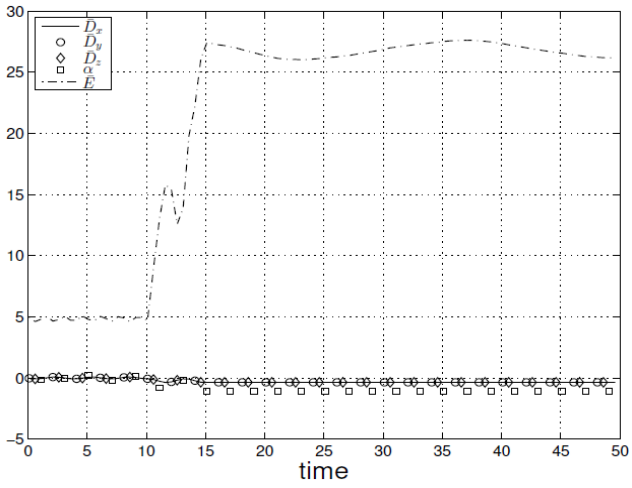

Fig. 4. Conservation of different quantities for the cube with prescribed $\boldsymbol{H} \times \boldsymbol{n}$ example

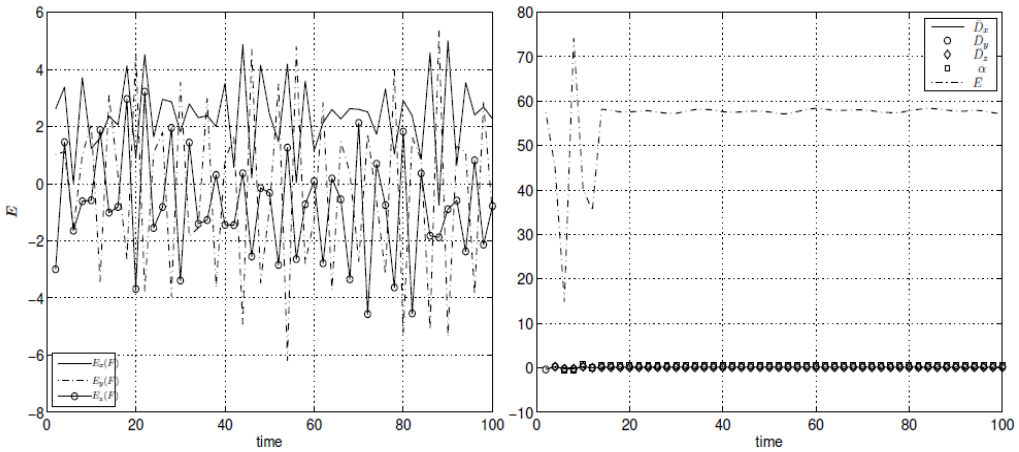

(a) $\boldsymbol{E}$ at $(x, y, z) = (1/2, 7/6, 3/2)$ (b) Conservation of different quantities

Fig. 5. Bounded nature of the solution and conservation of various quantities with a very large time step for the cube with boundary-prescribed $\boldsymbol{H}$ problem

3.3 An axisymmetric radiation problem

An axisymmetric analytical solution to the transient Maxwell equations on an unbounded domain expressed in terms of spherical coordinates r-θ-ϕ is

$$
\begin{aligned}
E_r &= E_\theta = 0, \\
E_\phi &= P_n^{(1)}(\cos\theta)\left[j_n(kr)\cos(\omega t) + y_n(kr)\sin(\omega t)\right], \\
H_\phi &= 0, \\
H_r &= \frac{n}{\mu\omega r\sin\theta}\left(P_n^{(1)}(\cos\theta)\cos\theta - P_{n+1}^{(1)}(\cos\theta)\right)\left[j_n(kr)\sin(\omega t) - y_n(kr)\cos(\omega t)\right], \\
H_\theta &= \frac{P_n^{(1)}(\cos\theta)}{\mu\omega rc}\big\{\left[\omega r y_{n+1}(kr) - c(n+1)y_n(kr)\right]\cos(\omega t) \\
&\quad - \left[\omega r j_{n+1}(kr) - c(n+1)j_n(kr)\right]\sin(\omega t)\big\},
\end{aligned}
\tag{3.3}
$$

where n is any integer, j_n and y_n denote the spherical Bessel functions of the first and second kind, and $P_n^{(m)}$ denote the associated Legendre polynomials. In the limit as θ tends to 0 or π, we have $E_\phi = H_\theta = 0$ and

$$
\begin{aligned}
\lim_{\theta\to 0} H_r &= \frac{n(n+1)}{\mu\omega r}\left[j_n(kr)\sin(\omega t) - y_n(kr)\cos(\omega t)\right], \\
\lim_{\theta\to \pi} H_r &= \frac{(-1)^n n(n+1)}{\mu\omega r}\left[j_n(kr)\sin(\omega t) - y_n(kr)\cos(\omega t)\right].
\end{aligned}
$$

The domain that we choose for our simulation is a hollow sphere of inner and outer radii a and R_∞, respectively (see Fig. 6). We have used a mesh of $n_r \times n_\theta = 1 \times 6$ elements for the FEM discretization. We prescribe an absorbing boundary condition on the boundary at R_∞, and prescribe $\bar{\boldsymbol{H}}$ on the inner boundary as per Eqns. (3.3). We have used $n = 1$, $\mu_r = 1$, $\epsilon_r = 1$, $ka = 10$ and $kR_\infty = 10.5$. Fig. 7 shows the almost perfect match obtained between the analytical (A) and FEM (F) solutions at two points.

3.4 Transverse Magnetic (TM) solution of the Maxwell equations

A transverse magnetic (along r) solution of the Maxwell equations, which is derived from the harmonic solution given in [36], is given by

$$
\begin{aligned}
E_r &= \frac{\omega n(n+1)}{kr}\sin(m\phi)P_n^{(m)}(\cos\theta)\left[j_n(kr)\sin(\omega t) - y_n(kr)\cos(\omega t)\right], && \text{(3.4a)} \\
E_\theta &= t_1 t_2\left[t_4\cos(\omega t) - t_5\sin(\omega t)\right], && \text{(3.4b)} \\
E_\phi &= -t_3\left[t_4\cos(\omega t) - t_5\sin(\omega t)\right], && \text{(3.4c)} \\
H_r &= 0, && \text{(3.4d)} \\
H_\theta &= \frac{\omega r t_3}{c\mu}\left[j_n(kr)\cos(\omega t) + y_n(kr)\sin(\omega t)\right], && \text{(3.4e)} \\
H_\phi &= \frac{\omega r t_1 t_2}{c\mu}\left[j_n(kr)\cos(\omega t) + y_n(kr)\sin(\omega t)\right], && \text{(3.4f)} \\
A_r &= \frac{n(n+1)}{kr}\sin(m\phi)P_n^{(m)}(\cos\theta)\left[j_n(kr)\cos(\omega t) + y_n(kr)\sin(\omega t)\right], && \text{(3.4g)} \\
A_\theta &= -\frac{t_1 t_2}{\omega}\left[t_5\cos(\omega t) + t_4\sin(\omega t)\right], && \text{(3.4h)} \\
A_\phi &= \frac{t_3}{\omega}\left[t_5\cos(\omega t) + t_4\sin(\omega t)\right], && \text{(3.4i)} \\
\psi &= 0, && \text{(3.4j)}
\end{aligned}
$$

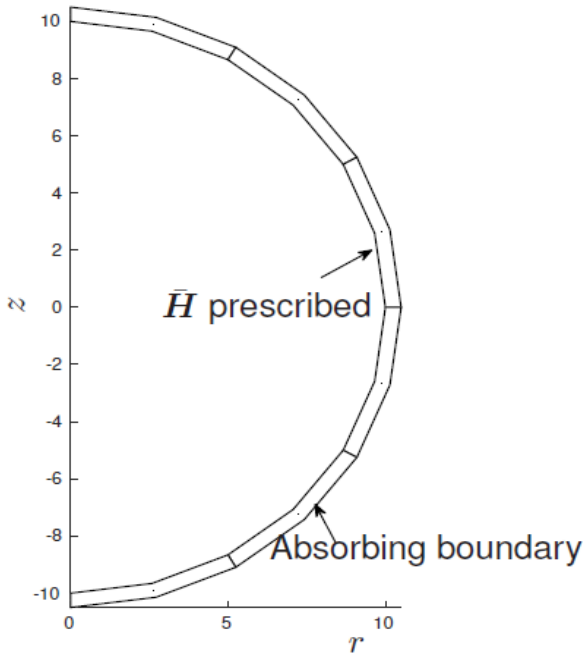

Fig. 6. Mesh for the axi-symmetric radiation problem

where m and n are any integers, and

$$
\begin{aligned}
t_1 &= \frac{\sin(m\phi)}{r\sin\theta}, \\
t_2 &= (n+1)\cos\theta P_n^{(m)}(\cos\theta) + (m-n-1)P_{n+1}^{(m)}(\cos\theta), \\
t_3 &= \frac{m\cos(m\phi)P_n^{(m)}(\cos\theta)}{r\sin\theta}, \\
t_4 &= c(n+1)y_n(kr) - \omega r y_{n+1}(kr), \\
t_5 &= c(n+1)j_n(kr) - \omega r j_{n+1}(kr).
\end{aligned}
$$

We have the following limiting values for $m = n = 1$:

$$
\begin{aligned}
E_\theta|_{\theta\to 0} &= [t_6\cos(\omega t) - t_7\sin(\omega t)]\,\omega\sin\phi, & E_\phi|_{\theta\to 0} &= [t_6\cos(\omega t) - t_7\sin(\omega t)]\,\omega\cos\phi, \\
H_\theta|_{\theta\to 0} &= [t_8\cos(\omega t) + t_9\sin(\omega t)]\,t_{10}\cos\phi, & H_\phi|_{\theta\to 0} &= -[t_8\cos(\omega t) + t_9\sin(\omega t)]\,t_{10}\sin\phi, \\
A_\theta|_{\theta\to 0} &= -[t_6\sin(\omega t) + t_7\cos(\omega t)]\sin\phi, & A_\phi|_{\theta\to 0} &= -[t_6\sin(\omega t) + t_7\cos(\omega t)]\cos\phi, \\
E_\theta|_{\theta\to \pi} &= -E_\theta|_{\theta\to 0}, & E_\phi|_{\theta\to \pi} &= E_\phi|_{\theta\to 0}, \\
A_\theta|_{\theta\to \pi} &= -A_\theta|_{\theta\to 0}, & A_\phi|_{\theta\to \pi} &= A_\phi|_{\theta\to 0}, \\
H_\theta|_{\theta\to \pi} &= H_\theta|_{\theta\to 0}, & H_\phi|_{\theta\to \pi} &= -H_\phi|_{\theta\to 0},
\end{aligned}
$$

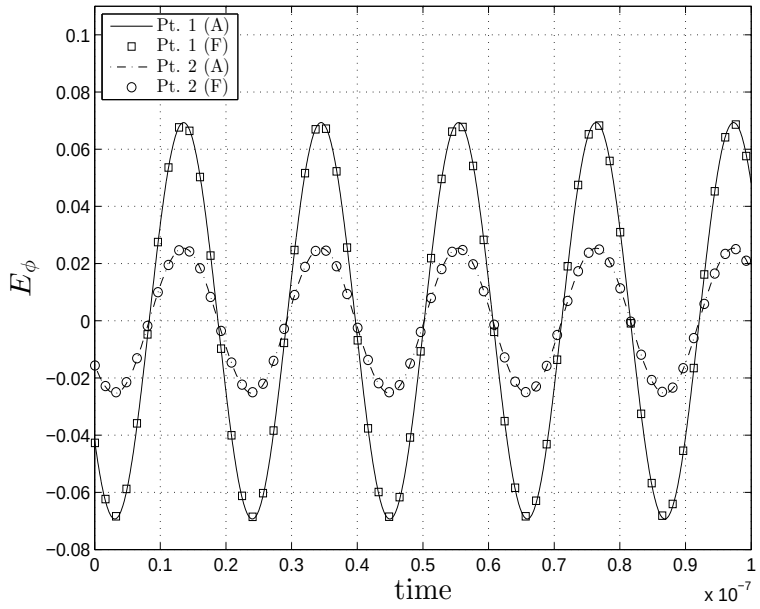

Fig. 7. Time variation of electric field at Point 1 with $(r, \theta) = (10.25, 45^\circ)$, and Point 2 with $(r, \theta) = (10.25, 165^\circ)$ in the axisymmetric radiation problem

where

$$t_6 = \frac{2}{kr} y_1(kr) - y_2(kr), \qquad t_7 = \frac{2}{kr} j_1(kr) - j_2(kr),$$
$$t_8 = kr\cos(kr) - \sin(kr), \qquad t_9 = kr\sin(kr) + \cos(kr),$$
$$t_{10} = \frac{\omega}{\mu c k^2 r^2}.$$

We again choose the domain to be a hollow sphere with inner radius a and outer radius R_∞. We enforce the absorbing boundary condition at the outer radius, while at the inner radius we prescribe the magnetic field $\boldsymbol{H}$ as per Eqn. (3.4). We choose $ka = 5$, $kR_\infty = 15$, $\mu_r = 1$, $\epsilon_r = 1$, $m = 1$ and $n = 1$ for our simulations. The domain is modelled with a $4 \times 6 \times 12$ (in the r-θ-ϕ directions) mesh of 27-node brick elements. Fig. 8 shows the results upto 2×10^{-8} sec obtained using $t_\Delta = 2 \times 10^{-10}$ sec. We again see an almost perfect correspondence between the analytical (A) and FEM (F) solutions for both the near- and far-field points.

3.5 Scattering from an empty box

Consider a wave incident on an empty box with $\mu_r = 1, \epsilon_r = 1$ [10]. The incident wave is given by

$$\boldsymbol{E}_{\text{inc}} = 2\{t - t_0 - \hat{\boldsymbol{k}} \cdot (\boldsymbol{r} - \boldsymbol{r}_0)/c\} \exp\left[-\frac{\{t - t_0 - \hat{\boldsymbol{k}} \cdot (\boldsymbol{r} - \boldsymbol{r}_0)/c\}^2}{\tau^2}\right] \hat{\boldsymbol{E}}, \tag{3.5}$$

where the parameters $t_0, \boldsymbol{r}_0$ and τ define a temporal reference point, a spatial reference point and the pulse shape, respectively. The domain is the empty box with dimensions (in meters) of $1.0 \times 0.5 \times 0.75$. An $\boldsymbol{H}$ field consistent with $\boldsymbol{E}_{\text{inc}}$ is applied on the entire boundary of the domain.

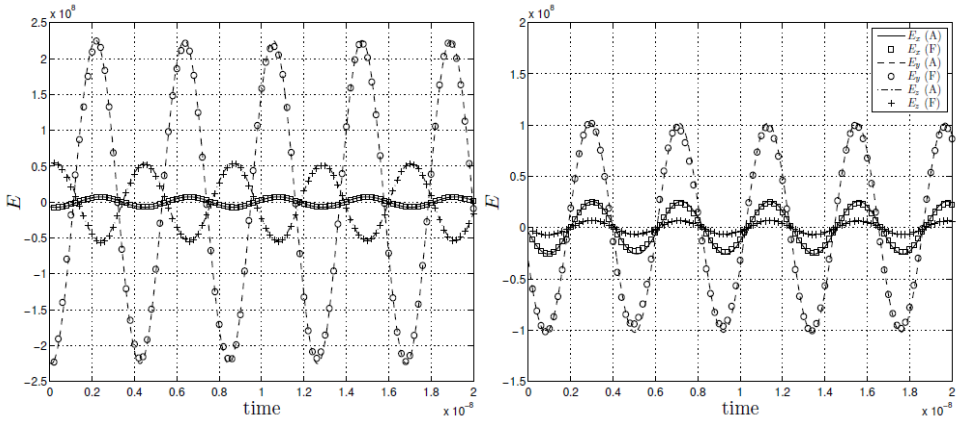

(a) $kr = 6.25$, $\theta = 15°$, $\phi = 120°$ (b) $kr = 13.75$, $\theta = 105°$, $\phi = 165°$

Fig. 8. Time variation of the electric field for the transverse magnetic field problem

The values of the parameters are chosen to be the same as in [10], namely, $\hat{\boldsymbol{k}} = \hat{\boldsymbol{y}}$, $\hat{\boldsymbol{E}} = \hat{\boldsymbol{z}}$, $\epsilon_r = 1$, $\mu_r = 1$, $x_0 = 0.5$, $y_0 = 0.5$, $z_0 = 0.375$, $t_0 = 25.99$ ns and $\tau = 5.25$ ns. The domain is modelled with a $4 \times 2 \times 3$ (along the x, y and z directions) mesh of 27-node brick elements, and the time-step is taken as 1 ns. The time variation of the $\boldsymbol{E}$ field upto 5×10^{-8} sec obtained using the proposed

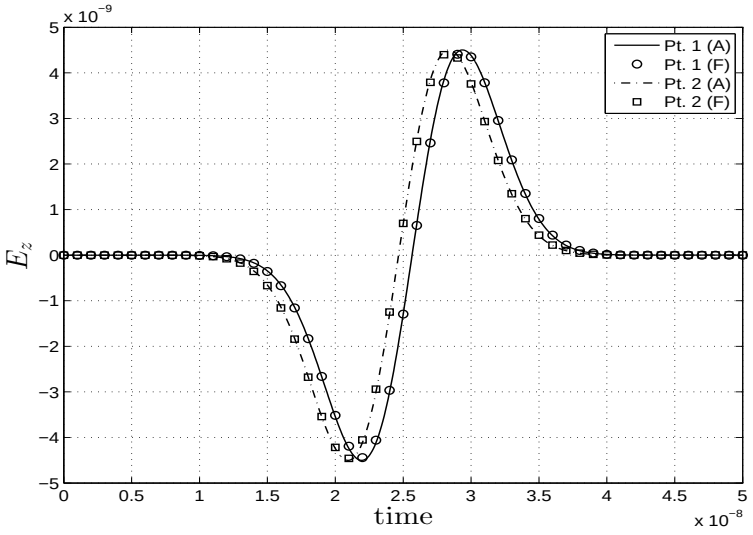

Fig. 9. Time variation of the electric field at Points 1 $(0.17, 0.4, 0.16)$ and 2 $(0.8, 0.1, 0.6)$ in the scattering from an empty box problem.

method (F) is plotted along with the analytical results (A) for two points with coordinates (x, y, z) given by $(0.17, 0.4, 0.16)$ and $(0.8, 0.1, 0.6)$ in Fig. 9. Again, the good correspondence between the proposed method and the analytical solution is evident.

3.6 Scattering from a conducting sphere

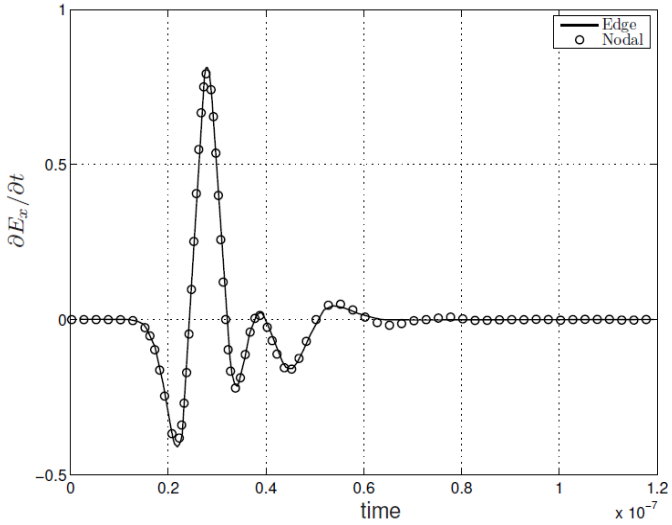

Fig. 10. Time variation of $\partial E_x/\partial t$ at $(0.33, -1.03, -0.45)$ for the scattering from a conducting sphere example

An incident wave of the form (3.5) impinges on a conducting sphere of radius 0.8 m with pulse parameters given by $\hat{\boldsymbol{k}} = \hat{\boldsymbol{z}}$, $\hat{\boldsymbol{E}} = \hat{\boldsymbol{x}}$, $t_0 = 25.99$ ns, $\boldsymbol{r}_0 = -1.2\hat{\boldsymbol{z}}$ m and $\tau = 5.25$ ns [6]. The computational domain is truncated at $R_\infty = 3.8$ m, and modelled with a $8 \times 8 \times 10$ (r-θ-ϕ) mesh of 27-node brick and 18-node wedge elements. The total number of nodes in the domain is 4794. The time step is taken to be 5×10^{-10} sec. For the time variation of $\partial E_x/\partial t$ at $(0.33, -1.03, -0.45)$, the almost perfect match between the result obtained using edge elements in [6], and our conserving strategy is evident from Fig. 10.

3.7 Scattering from a dielectric sphere

Consider a Neumann pulse as given in Eqn. (3.5) incident on a dielectric sphere of radius 0.5 m having $\mu_r = 1$ and $\epsilon_r = 6.0$ [5]. The parameters in the Neumann pulse are chosen to be $\hat{\boldsymbol{E}} = \hat{\boldsymbol{x}}$, $\hat{\boldsymbol{k}} = \hat{\boldsymbol{z}}$, $t_0 = 25.9$ ns, $\boldsymbol{r}_0 = -1.3\hat{\boldsymbol{z}}$ and $\tau = 5.25$ ns. The computational domain is truncated at $R_\infty = 2$ m and is modeled with 10 node tetrahedral elements. In order to show that our strategy converges with respect to mesh refinement, we use two meshes. The coarse and fine meshes used have 10696 elements/14798 nodes and 24342 elements/33832 nodes, respectively. The respective time-steps used for the coarse and the fine meshes are 0.5 ns and 0.2 ns. The plot of the time variation of $\boldsymbol{E} \cdot \boldsymbol{t}$ at $(-0.04, -0.07, -0.72)$ with $\boldsymbol{t} = 0.96\hat{\boldsymbol{x}} + 0.26\hat{\boldsymbol{y}} + 0.13\hat{\boldsymbol{z}}$ and at $(0.05, 0.05, -0.96)$ with $\boldsymbol{t} = -0.89\hat{\boldsymbol{x}} - 0.08\hat{\boldsymbol{y}} + 0.44\hat{\boldsymbol{z}}$ is depicted in Fig. 11 which again shows the excellent match between the coarse and fine mesh results, and the results obtained using edge elements in [5].

3.8 Scattering from a coated dielectric sphere

An incident Neumann pulse with the same parameters as in the previous example impinges on a conducting sphere of radius 0.3 m with a coating of dielectric material having thickness of 0.2 m, and $\mu_r = 1$ and $\epsilon_r = 8$ [5]. The computational domain is again taken to be a sphere with $R_\infty = 2$

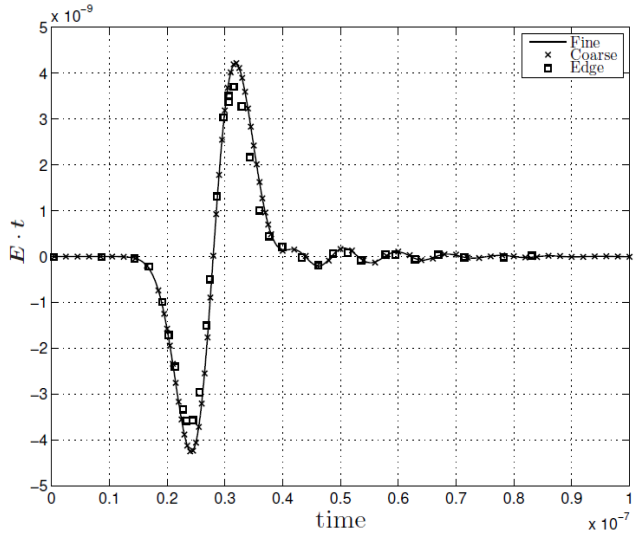

(a) $\boldsymbol{E} \cdot t$ at $(-0.04, -0.07, -0.72)$ with $t = 0.96\hat{x} + 0.26\hat{y} + 0.13\hat{z}$

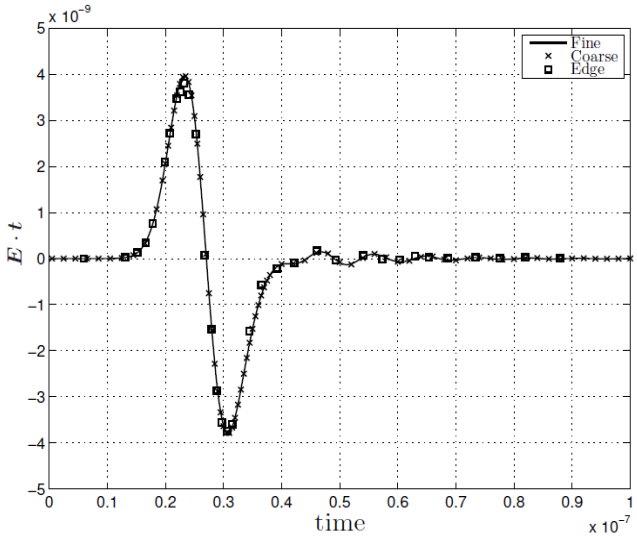

(b) $\boldsymbol{E} \cdot t$ at $(0.05, 0.05, -0.96)$ with $t = -0.89\hat{x} - 0.08\hat{y} + 0.44\hat{z}$

Fig. 11. Time variation of $\boldsymbol{E} \cdot \boldsymbol{t}$ for the scattering from a dielectric sphere example

m. A coarse mesh with 13313 nodes/9414 elements and 0.5 ns time-step and a fine mesh with 32243 nodes/22849 elements and 0.25 ns time-step are used to conduct the analysis. The time variation of E_x at $(0.077, 0.076, -0.85)$ and $\boldsymbol{E} \cdot \boldsymbol{t}$ at $(0.02, -0.088, -0.76)$ with $\boldsymbol{t} = 0.94\hat{\boldsymbol{x}} + 0.32\hat{\boldsymbol{y}} + 0.1\hat{\boldsymbol{z}}$ is shown in Fig. 12. Once again the extremely good match between our coarse and fine mesh results, and the results obtained using edge elements in [5] is evident from the figure.

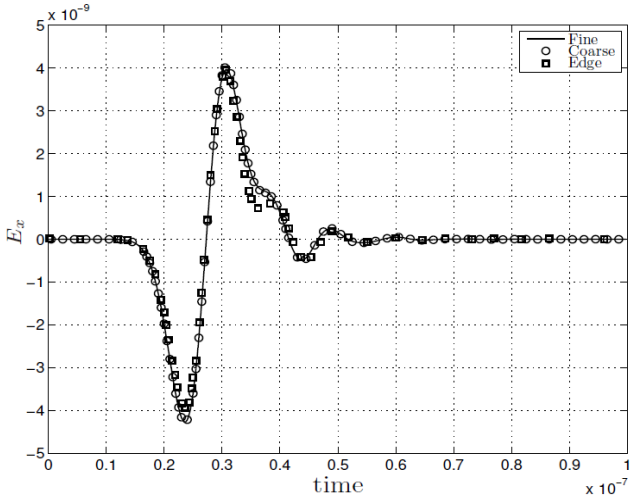

(a) E_x at $(0.077, 0.076, -0.85)$

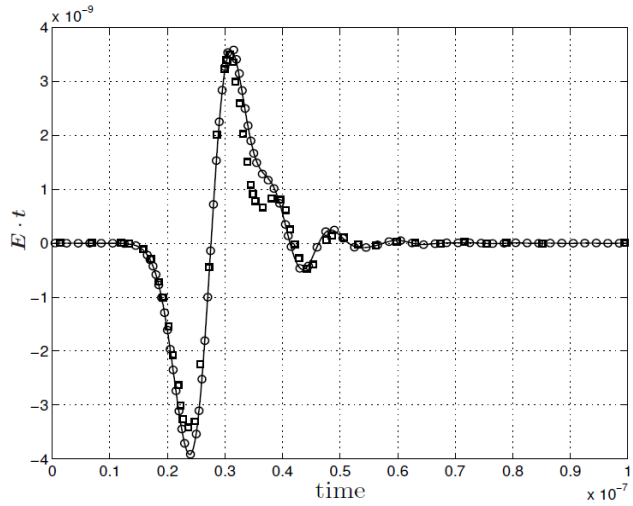

(b) $E \cdot t$ at $(0.02, -0.088, -0.76)$ with $t = 0.94\hat{x} + 0.32\hat{y} + 0.1\hat{z}$

Fig. 12. Time variation of the electric field for the scattering from a coated dielectric sphere example

3.9 Scattering from a conducting L shape domain

An incident Neumann pulse as given by Eqn. (3.5) with parameters $\hat{\boldsymbol{E}} = \cos(135^\circ)\hat{\boldsymbol{x}} + \sin(135^\circ)\hat{\boldsymbol{y}}$, $\hat{\boldsymbol{k}} = \cos(225^\circ)\hat{\boldsymbol{x}} + \sin(225^\circ)\hat{\boldsymbol{y}}$, $t_0 = 25.9$ ns, $\boldsymbol{r}_0 = 0.6\hat{\boldsymbol{x}} + 1.4\hat{\boldsymbol{y}}$ and $\tau = 5.25$ ns impinges on an L-shaped domain as shown in Fig. 13. The computational domain is a sphere of radius $R_\infty = 2.5$ m. The problem is modeled with 10-node tetrahedral elements. The center point of the left-bottom edge of the L-shape is chosen as the origin of the domain. Coarse and fine meshes with 16419 and 35947 nodes, and time-steps of 0.5 ns and 0.2 ns, respectively, are used to model this problem. Fig. 14 shows the variation of E_x at $(0.55, 0.89, 0.25)$ for both the coarse and fine meshes. The

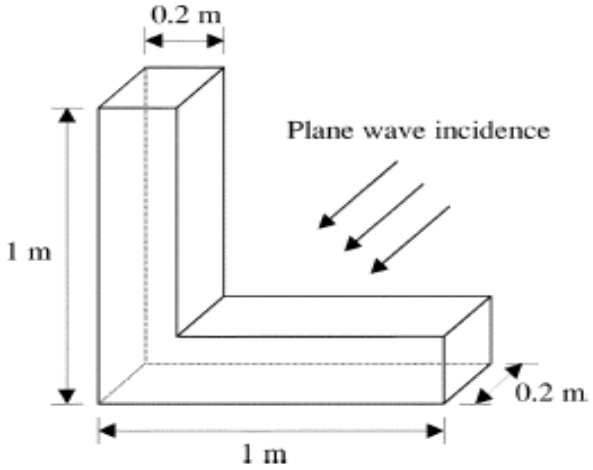

Fig. 13. Geometry of the L shape domain

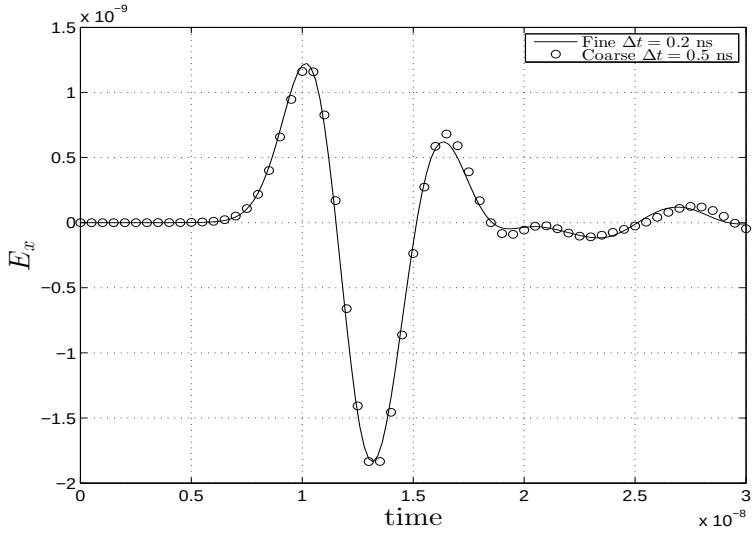

Fig. 14. The variation of E_x with time at $(0.55, 0.89, 0.25)$ for the conducting L-shaped domain problem.

convergence of the result with respect to mesh and time refinement is evident.

3.10 Scattering from a set of conducting spheres

An incident pulse as given by Eqn. (3.6) with parameters $\hat{\boldsymbol{E}} = \hat{\boldsymbol{x}}$, $\hat{\boldsymbol{k}} = \hat{\boldsymbol{z}}$, $t_0 = 13.66$ ns, $\boldsymbol{r}_0 = 0$, $f = 500 \times 10^6$ and $\tau = 2.6$ ns impinges on a set of three conducting spheres of radius 0.1 with

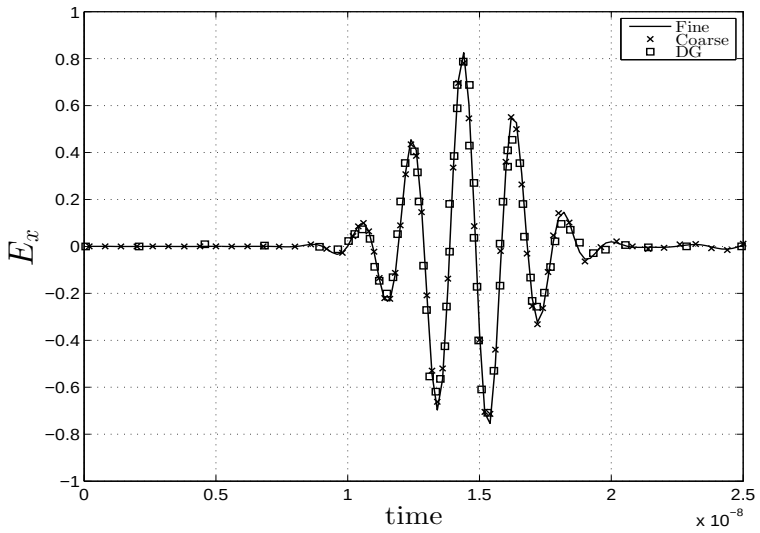

Fig. 15. Scattered E_x at origin for the set of conducting spheres

centers at $(0.2, 0, 0)$, $(-0.1, 0.173, 0)$ and $(-0.1, -0.173, 0)$ [22].

$$\boldsymbol{E}_{\text{inc}} = \cos\left[2\pi f\{t - t_0 - \hat{\boldsymbol{k}} \cdot (\boldsymbol{r} - \boldsymbol{r}_0)/c\}\right] \exp\left[-\frac{\{t - t_0 - \hat{\boldsymbol{k}} \cdot (\boldsymbol{r} - \boldsymbol{r}_0)/c\}^2}{\tau^2}\right] \hat{\boldsymbol{E}}. \tag{3.6}$$

The computational domain is chosen to be a sphere with radius $R_\infty = 0.6$. Coarse and fine meshes with 20335 and 30091 nodes, respectively are used for conducting the analysis. The time-step is chosen to be 0.2 ns. Fig. 15 shows the convergence of the result with mesh refinement and the good match of the converged result with that obtained in [22] using a discontinuous Galerkin (DG) method.

4 Conclusion

Just as linear and angular momentum and total energy are conserved in the absence of loading and dissipation in structural mechanics problems, we have derived a set of parameters that are conserved in the absence of electromagnetic loading (see Eqns. (2.14)). Next, using a potential formulation under a nodal finite element framework, we have formulated a time-stepping strategy that mimics these continuum conservation properties. The strategy has been formulated for both electromagnetic radiation and scattering problems for interior and exterior domain problems. It is, in general, difficult to model sharp edges and corners within the context of nodal finite elements. We have shown how the strategy can be suitably modified in the presence of sharp edges and corners so that singularities can be captured. Numerous problems involving both radiation and scattering from conducting bodies and dielectrics, and bodies with sharp corners and edges such as an L-shaped domain have been solved, and the solutions compared against either analytical solutions or numerical solutions obtained using other strategies in the literature in order to demonstrate the robustness and efficiency of the proposed strategy.

Competing Interests

Authors have declared that no competing interests exist.

References

[1] Yee KS. Numerical solution of initial boundary value problems involving Maxwell's equations in isotropic media. IEEE transactions on Antennas and Propagation. 1966;14(8):302-307.

[2] Taflove A. Computational electrodynamics: The finite-difference time-domain method. MA, Artech House, Boston; 1995

[3] Tsai HP, Wang Y, Itoh T. An unconditionally stable extended (USE) finite-element time-domain solution of active nonlinear microwave circuits using perfectly matched layers. IEEE Transactions on Microwave Theory and Technique. 2002;50(10):2226-2232.

[4] Lee JF. WETD-A finite element time-domain approach for solving Maxwell's equations. IEEE Microwave and Guided wave letters. 1994;4(1):11-13.

[5] Jiao D, Jin JM, Michielssen E, Riley DJ. Time-domain finite-element simulation of three-dimensional scattering and radiation problems using perfectly matched layers. IEEE transactions on Antennas and Propagation. 2003;51(2):296-305.

[6] Jiao D, Ergin A, Shanker B, Michielssen E, Jin JM. A fast higher-order time-domain finite element-boundary integral method for 3-D electromagnetic scattering analysis. IEEE transactions on Antennas and Propagation. 2002;50(9):1192-1202.

[7] Qiu ZJ, Xu JD, Wei G, Hou XY. An improved timedomain finite element- boundary integral scheme for electromagnetic scattering from 3D objects. Progress In Electromagnetics Research. 2007;75:119-135.

[8] Faghihi F, Heydari H. Combination of timedomain finite element-boundary integral with timedomain physical optics for calculation of electromagnetic scattering of 3d structures. Progress In Electromagnetics Research. 2008;79:463-474.

[9] Artzuri WA. Improving the Newmark time integration scheme in finite element time domain methods. IEEE Microwave and Wireless Components Letters. 2005;15(12):898-900.

[10] Jiao D, Jin JM. Three-dimensional orthogonal vector basis functions for time-domain finite element solution of vector wave equations. IEEE transactions on Antennas and Propagation. 2003;51(1):59-66.

[11] Lee JF, Lee R, Cangellaris A. Time-domain finite-element methods. IEEE transactions on Antennas and Propagation. 1997;45(3):430-442.

[12] Wong MF, Picon O, Hanna VF. A finite element method based on whitney forms to solve Maxwell equations in the time domain. IEEE Transactions on Magnetics. 1995;31(3):1618-1621.

[13] Movahhedi M, Abdipour A, Nentchev A, Dehghan M, Selberherr S. Alternating-direction implicit formulation of the finite-element time-domain method. IEEE Transactions on Microwave Theory and Technique. 2007;55(6):1322-1331.

[14] Chen RS, Du L, Ye Z, Yang Y. An efficient algorithm for implementing the Crank-Nicholson scheme in the Mixed Finite-element time-domain method. IEEE transactions on Antennas and Propagation. 2009;57(10):3216-3222.

[15] Rodrigue G, White D. A vector finite element time-domain method for solving Maxwell's equations on unstructured Hexahedral Grids. SIAM Journal on Scientific Computing. 2001;23(3):683-706.

[16] Sekine T, Asai H. Mixed finite element time domain method based on iterative leapfrog scheme for fast simulations of electromagnetic problems. IEEE International Symposium on Electromagnetic Compatibility (EMC). 2011;596-601.

[17] Rieben RN, Rodrigue GH, White DA. A high order mixed vector finite element method for solving the time dependent Maxwell equations on unstructured grids. Journal of Computational Physics. 2005;204(2):490-519.

[18] Cangellaris AC, Lin CC, Mei KK. Point-matched time domain finite element methods for electromagnetic radiation and scattering. IEEE transactions on Antennas and Propagation. 1987;AP-35(10):1160-1173.

[19] Jiao D, Lu M, Michielssen E, Jin JM. A fast time-domain finite element-boundary integral method for electromagnetic analysis. IEEE Transactions on Antennas and Propagation. 2001;49(10):1453-1461.

[20] Lee R, Madsen NK. A mixed finite element formulation for maxwell's equations in the time domain. Journal of Computational Physics. 1990;88(2):284-304.

[21] Monk P. A comparison of three mixed methods for the time-dependent Maxwell's equations. SIAM Journal on Scientific and Statistical Computing. 1992;13(5):1097-1122.

[22] Taube A, Dumbser M, Munz CD, Schneider R. A high-order discontinuous Galerkin method with time-accurate local time stepping for the Maxwell equations. International Journal of Numerical Modelling: Electronic Networks, Devices and Fields. 2009;22(1):77-103.

[23] Tobon LE, Ren Q, Liu QH. A new efficient 3D discontinuous Galerkin Time Domain (DGTD) method for large and multiscale electromagnetic simulations. Journal of Computational Physics. 2015;283:374-387.

[24] Li P, Shi Y, Jiang LJ, Bagci H. A hybrid time-domain discontinuous Galerkin-boundary integral method for electromagnetic scattering analysis. IEEE Transactions on Antennas and Propagation. 2014;62(5):2841-2846.

[25] Lou Z, Jin JM. A novel dual-field time-domain finite-element domain-decomposition method for computational electromagnetics. IEEE Transactions on Antennas and Propagation. 2006;54(6):1850-1862.

[26] Lou Z, Jin JM. A dual-field domain-decomposition method for the time-domain finite-element analysis of large finite arrays. Journal of Computational Physics. 2007;222(1):408-427.

[27] Lu ZQ, An X, Hong W. A fast domain decomposition method for solving three-dimensional large-scale electromagnetic problems. IEEE Transactions on Antennas and Propagation. 2008;56(8):2200-2210.

[28] Lynch DR, Paulsen KD. Time-Domain Integration of the Maxwell Equations on Finite Elements. IEEE Transaction on Antennas and Propagation. 1990;38(12):1933-1942.

[29] Kole JS, Figge MT, Raedt HD. Unconditionally stable algorithms to solve the time-dependent Maxwell equations. Physical review E. 2001;64(6):66705.

[30] Chen W, Li X, Liang D. Energy-conserved splitting FDTD methods for Maxwell's equations. Numerische Mathematik. 2008;108(3):445-485.

[31] Jog CS, Nandy A. Conservation properties of the trapezoidal rule in linear time domain analysis of acoustics and structures. ASME J. Vibration Acoustics. 2015;137(2):021010.

[32] Richtmyer RD, Morthon KW. Difference Methods for Initial Value Problems. John Wiley & Sons., Newyork; 1967.

[33] Kuhl D, Crisfield MA. Energy-conserving and decaying algorithms in non-linear structural dynamics. International Journal for Numerical Methods in Engineering. 1999;45(5):569-599.

[34] Bardi I, Biro O, Preis K. Finite element scheme for 3D cavities without spurious modes. IEEE Transaction on Magnetics. 1991;27(5):4036-4039.

[35] Jog CS, Nandy A. Mixed finite elements for electromagnetic analysis. Computers and Mathematics with Applications. 2014;68(8):887-902.

[36] Nandy A, Jog CS. An amplitude finite element formulation for electromagnetic radiation and scattering. Computer and Mathematics with Application. 2016;71(7):1364-1391.

[37] Costabel M, Dauge M. Weighted regularization of Maxwell equations in polyhedral domains. Numerische Mathematik. 2002;93(2):239-277.

[38] Otin R. Regularized Maxwell equations and Nodal finite elements for electromagnetic field computations. Electromagnetics. 2010;30(1-2):190-204.

[39] Otin R. ERMES: A nodal-based finite element code for electromagnetic simulations in frequency domain. Computer Physics Communications. 2013;184(11):2588-2595.

[40] Jog CS, Agrawal M, Nandy A. The time finite element as a robust general scheme for solving nonlinear dynamic equations including chaotic systems. Applied Mathematics and Computation. 2016;279:43-61.

[41] Ma C. Finite-element method for time-dependent Maxwell's equations based on an explicit-magnetic-field scheme. Journal of Computational and Applied Mathematics. 2006;194(2):409-424.

Peer-review history:
The peer review history for this paper can be accessed here (Please copy paste the total link in your browser address bar)
http://www.sciencedomain.org/review-history/23334